



Κουφονήσια

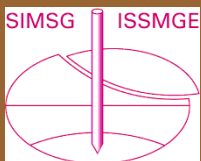


ΕΛΛΗΝΙΚΗ  
ΕΠΙΣΤΗΜΟΝΙΚΗ  
ΕΤΑΙΡΕΙΑ  
ΕΔΑΦΟΜΗΧΑΝΙΚΗΣ  
& ΓΕΩΤΕΧΝΙΚΗΣ  
ΜΗΧΑΝΙΚΗΣ

# Τα Νέα της Ε Ε Ε Ε Γ Μ

139  
B

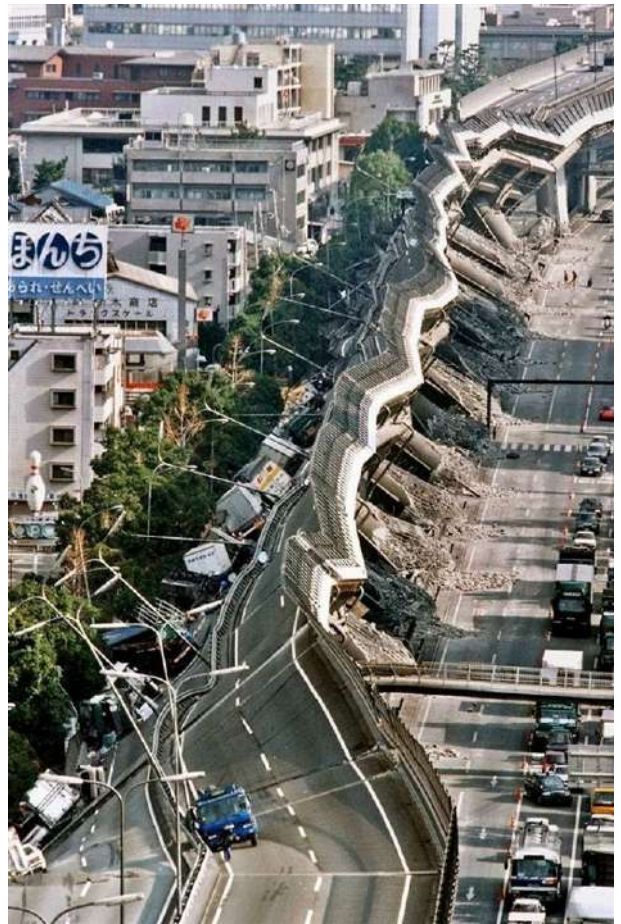
Αρ. 139B – ΙΟΥΝΙΟΣ 2020



Ίλος – Χώρα

## ΠΕΡΙΕΧΟΜΕΝΑ

Άρθρα	3
- ICE Publishing Awards	
- Pore water pressure and total horizontal stress response to EPBM tunnelling in London Clay	4
- Rehabilitation of Brougham Castle Bridge, UK	21



Οικοδομή του 2005, οροφή υπογείου



Each year the ICE Publishing Awards celebrate authors from both industry and academia who have produced work judged by their peers to be of exceptional quality and benefit to the civil engineering, construction and materials science community.

The panel said that this year's winning papers '*are all well written, relevant, and interesting*'. They cover projects from around the world and all aspects of civil and environmental engineering, and materials science.

#### Top three papers



[Pore water pressure and total horizontal stress response to EPBM tunnelling in London Clay](#), M. S. P. Wan, J. R. Standing, D. M. Potts and J. B. Burland, *Géotechnique*



[Downwind flow behaviours of cuboid-shaped obstacles: modelling and experiments](#), Karl An, Julian C. R. Hunt, and Jimmy C. H. Fung, *Engineering and Computational Mechanics*



[Rehabilitation of Brougham Castle Bridge](#), David Wiggins, Kiera Mudd and Matthew Healey, *Engineering History and Heritage*

## Pore water pressure and total horizontal stress response to EPBM tunnelling in London Clay

M. S. P. Wan, J. R. Standing, D. M. Potts, J. B. Burland

### Abstract

The ground response, in terms of surface and subsurface displacements, to twin-bore Crossrail tunnel construction beneath a research monitoring site in Hyde Park, London, using earth-pressure-balance machines (EPBMs) in London Clay, has recently been reported in two companion papers by the authors. This third paper presents and discusses corresponding changes in pore water pressure and total horizontal stress measured using multi-level piezometers and pushed-in spade cells. The three papers together provide a comprehensive and completely unique field monitoring case history of the short-term ground response to EPBM tunnelling in London Clay, making them invaluable for validating future numerical analyses. The fully grouted vibrating-wire piezometers were able to measure the rapid pore water pressure changes around the tunnels as they were constructed. Five distinct immediate pore water pressure responses are identified, induced by different stages of the tunnel drives as the EPBMs approached and passed the instruments. The responses are correlated with tunnel-boring machine operation variables and a postulated arching mechanism, identified for the first time through field measurements. The sense and magnitude of changes in horizontal total stress were reasonable and are correlated with overall pore water pressure changes. Both responses are linked where possible with measured subsurface displacements and generally correlate well, at least qualitatively. Limitations to the measurements and influencing factors are also discussed.

### BACKGROUND

Tunnel construction induces displacements, total stress changes and excess pore water pressures in the surrounding ground. In saturated ground of low permeability, the immediate response to the resulting changes in total stress is essentially undrained, causing rapid changes in pore water pressure. This is followed by a gradual drained response as pore water pressures equalise towards a steady state governed by both the far-field and soil-tunnel-lining interface drainage boundary conditions. Understanding the development of excess pore water pressures induced by tunnel construction is of significant interest to asset owners, engineers and researchers because: (a) long-term ground settlements are largely controlled by the dissipation of the excess pore water pressures; and (b) they provide a means of validating/calibrating complex numerical analyses modelling tunnels. Construction of the twin-bore Crossrail tunnels provided an opportunity to monitor the development of pore water pressure and total stress changes, in conjunction with ground displacements, during their construction by earth-pressure-balance machines (EPBMs) in London Clay.

Measurements of the development of pore water pressure and total stress induced by tunnelling in soft or stiff clays have not been reported in the literature as extensively as corresponding ground displacements. Published accounts of field pore water pressure measurements during shield tunnelling include those in soft clays in the UK ([Glossop, 1978](#)), Canada ([Palmer & Belshaw, 1980](#)), Singapore ([Lo et al., 1988](#); [Shirlaw & Doran, 1988](#)), China ([Yi et al., 1993](#); [Lee et al., 1999](#)) and Taiwan ([Hwang et al., 1995](#)). Pore water pressure measurements have also been taken in centrifuge test modelling of tunnelling in soft clay ([Mair, 1979](#); [Grant, 1998](#); [Dival et al., 2017](#)). More cases exist for tunnelling in London Clay with pore water pressure measurements taken at various sites: Regent's Park, central London, during hand-driven

open-shield tunnel construction ([Barratt & Tyler, 1976](#)); Heathrow, west London, during tunnel construction using the sprayed concrete lining method ([New & Bowers, 1994](#); [Clayton et al., 2000](#)); St. James's Park, central London, during and after open-face shield tunnelling ([Nyren, 1998](#)); West Ham, east London, during closed-face shield tunnelling ([Macklin & Field, 1999](#)); and at Dagenham, east of London, during EPBM tunnelling ([Standing & Selemetas, 2013](#)).

This paper focuses on the measured immediate ground response in terms of pore water pressure and total horizontal stress changes induced by the passage of the two Crossrail EPBMs in London Clay. Measuring pore water pressure changes at various elevations and offsets to tunnel construction is of significant interest as this can facilitate the understanding of the extent of the immediate response and the spatial distribution of the generated excess pore water pressures. At an instrumented 'greenfield' site in Hyde Park, London, pore water pressures and total stress changes were measured in the close vicinity of the Crossrail tunnel construction by: (a) multi-level vibrating-wire (VW) type piezometers installed in boreholes, and (b) pushed-in total stress spade cells (with built-in piezometers). These piezometers formed part of an extensive instrumentation and monitoring scheme for measuring the tunnelling-induced ground response. The short-term surface and subsurface ground displacements are presented and discussed respectively in two companion papers ([Wan et al., 2017a](#), [2017b](#)) and have, where possible, been correlated with the changes in pore water pressure and total stress.

During the assessment of the pore water pressure data in conjunction with the EPBM operation variables it became evident that a more realistic interpretation of the data could be achieved by postulating an arching mechanism around the shield as it advanced. Ground arching was defined and discussed by [Terzaghi \(1943\)](#) and although often associated with granular soils, it can equally develop in more continuum-like clay soils. Essentially the mechanism involves a yielding region of a soil mass (in the tunnelling context, that part moving into the face or tail skin region) where in the short term total stresses reduce, and a more stationary region around the yielding part of the soil mass, where total stresses increase. More recently, [Lee et al. \(2006\)](#) investigated an arching mechanism around tunnel excavation by finite-difference modelling and centrifuge modelling, while [Jiang & Yin \(2012\)](#) investigated the development of ground arching around tunnel excavation using the discrete-element method.

In low-permeability clays such as London Clay, a decrease/increase in total stress results, under undrained conditions, in a broadly equal decrease/increase in pore water pressure. Arching mechanisms are referred to when describing the piezometer and spade cell responses to tunnelling and are discussed more fully in the section entitled 'Mechanisms of EPBM tunnelling-induced pore water pressure changes and ground arching'. The results presented in this paper strongly suggest an arching mechanism, identified for the first time through field measurements, for an advancing EPBM in London Clay.

The Hyde Park field monitoring work formed part of an extensive research project investigating the effect of tunnelling on existing tunnels, which also involved in-tunnel measurements, structural testing of bolted cast-iron segments, numerical analyses and advanced laboratory soil testing ([Standing et al., 2015](#); [Avgerinos et al., 2016](#), [2017](#), [2018](#); [Afshan et al., 2017](#); [Tsiampousi et al., 2017](#); [Yu et al., 2017](#)). As with the second companion paper ([Wan et al., 2017b](#)), in this current paper the intention is to provide sufficient background information such that it can be read and understood independently of the companion papers. Many more details

relating to the Crossrail project, site geology, instrumentation layout and the EPBMs used can be found in them (especially [Wan et al. \(2017a\)](#)). These details have been omitted here in order to avoid needless repetition, but where necessary the reader is directed to appropriate sections and figures in the companion papers.

A primary intention of the three papers is to provide comprehensive, research-quality field-monitoring data, in conjunction with detailed information on the EPBMs, their progression and their operation variables, to enable those performing advanced numerical studies to be able to validate their analyses and calibrate their constitutive models. Detailed results from the soil testing of high-quality samples taken during the installation of instruments at Hyde Park are currently being written up in a separate paper.

## CROSSRAIL TUNNELLING WORK AND SITE GEOLOGY AND HYDROGEOLOGY

The westbound and eastbound Crossrail tunnel drives beneath Hyde Park were part of the western tunnelling section from the Royal Oak portal to Farringdon station. The Hyde Park research site was set up close to where the Crossrail tunnels pass beneath the existing Central Line tunnels under Bayswater Road, just east of Lancaster Gate underground station. The relative positions of the tunnels are shown in Fig. 1, their respective axis depths are about 24 m (Central Line) and 34.5 m (Crossrail) below ground level (mbgl).

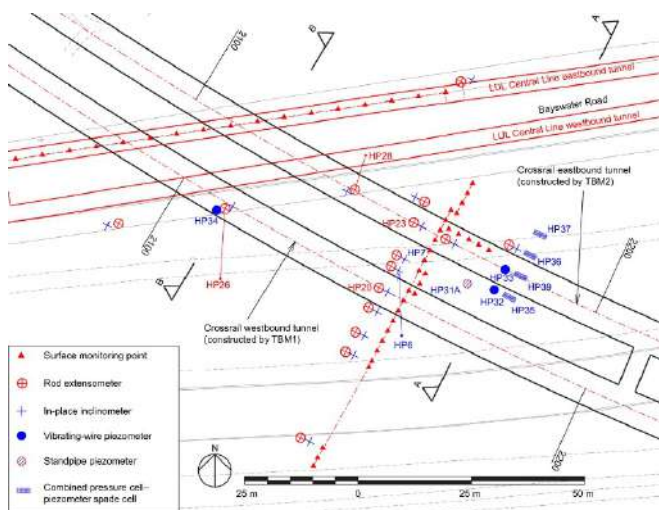


Fig. 1. Instrumentation layout plan

The EPBMs used to construct the Crossrail tunnels were 7.1 m in diameter with tapered shields of length 11 m. The tunnel lining rings, with inner and outer diameters of 6.2 m and 6.8 m, respectively, and length of 1.6 m, were formed of seven precast concrete bolted segments and a key-piece, erected within the shield body. The annulus void between the tunnel lining extrados and the excavated ground was filled with a two-part grout, usually termed the 'tail-skin grout' or 'tail grout'. Details of the EPBMs used are given by [Wan et al. \(2017a: Fig. 5 and pp. 423–424\)](#). Within the EPBMs comprehensive systems of instrumentation allowed operation variables to be monitored continuously.

The stratigraphy beneath the Hyde Park site is typical of central London with made ground and Terrace Gravels overlying the descending sequence of the London Clay Formation (LCF), Lambeth Group, Thanet Sand and Chalk bedrock. The detailed stratigraphy is shown and described by [Wan et al. \(2017a: Fig. 2\)](#) and that in the vicinity of the Central Line

tunnels (division B2 of the LCF) and the deeper Crossrail tunnels (crown in division B2 and invert within the more permeable A3ii) are marked in this paper on the cross-sections in Fig. 2. More detailed information on the LCF divisions is given by [King \(1981\)](#).

Two aquifers are present at the instrumented site, as reported by many authors (e.g. [Simpson et al., 1989](#)). The Terrace Gravels constitute the upper aquifer, and the combined lower granular units of the Lambeth Group (Upnor Formation), the Thanet Sand and Chalk the lower aquifer. These aquifers are separated by the LCF and, if present, the upper and lower mottled beds of the Lambeth Group. During borehole drilling for the installation of the instrumentation, the upper water table was established to be about 4–5 mbgl within the Thames Gravels, fluctuating by small degrees with season.

The deep water table was historically artesian but is now much lower owing to excessive abstraction activities in the early 1900s. Following the 'Gardit' (general aquifer research development and investigation team) strategy the water table is maintained below its natural level by controlled abstraction ([Jones, 2007](#)). As a result, the LCF is under-drained. An example of such a profile at Waterloo is given by [Wright \(2013\)](#) and was also observed at this site in the steady-state pore-water pressure profile measured by one of the 'greenfield' multi-level VW piezometers and the standpipe piezometers (see [Fig. 3\(a\)](#)).

## FIELD MONITORING

### Field instrumentation layout and installation

The instrumentation layout shown in [Fig. 1](#) was designed specifically to monitor the subsurface ground responses induced by the construction of the westbound and eastbound tunnels. Installations for measuring pore water pressures include three boreholes containing multi-level VW piezometers, and one with a conventional standpipe piezometer. There are also four boreholes with combined total stress transducer-piezometer spade cells. Cross-sections A–A and B–B marked in [Fig. 1](#) indicate the relative positions of the different types of piezometer sensors and the Crossrail tunnels and are shown in [Figs 2\(a\)](#) and [2\(b\)](#).

Within Hyde Park, two piezometer boreholes (HP32 and HP33), with six piezometer sensors at various depths in each, were installed above and adjacent to the Crossrail eastbound tunnel. One spade cell (HP39) was installed 1.5 m directly above the same eastbound tunnel crown and three others (HP35, HP36 and HP37) either side of it, all being at tunnel axis level ([Fig. 2\(a\)](#)). Under the southern pavement of Bayswater Road, there is one multi-level piezometer borehole (HP34), containing six sensors, directly above the Crossrail westbound tunnel (at depths down to 2 m above crown level) and at a horizontal offset of 5 m from the existing Central Line westbound tunnel extrados ([Fig. 2\(b\)](#)).

The multi-level piezometers were installed in the boreholes using a fully grouted method where the VW sensors (manufactured by Soil Instruments Ltd), equipped with high-air-entry filters and having a measurement range of 300 kPa or 500 kPa, were fixed at pre-determined levels within the borehole before backfilling with a suitable cement–bentonite grout. [Wan & Standing \(2014a\)](#) discuss in detail the installation, including the selection of suitable grout mix proportions. [Wan & Standing \(2014b\)](#) present the background and pre-construction pore water pressures measured by these piezometers and the resulting steady-state pore water pressure profiles at the site. Good agreement between the measurements from the standpipe piezometer (HP31A) and the VW

piezometers was demonstrated. Detailed analysis of the results also revealed the potential influence of claystones present in the LCF on the groundwater regime and the performance of the multi-level piezometers. It was established that the three bottom-most piezometer sensors in HP33 were hydraulically interconnected due to a high concentration of claystones over the relevant depth range. [Wan & Standing](#)

(2014b) also present a reduced pore water pressure profile at the current site measured close to the existing Central Line tunnels (constructed with segmental cast-iron linings in the nineteenth century), suggesting that they have been draining the surrounding ground (LCF).

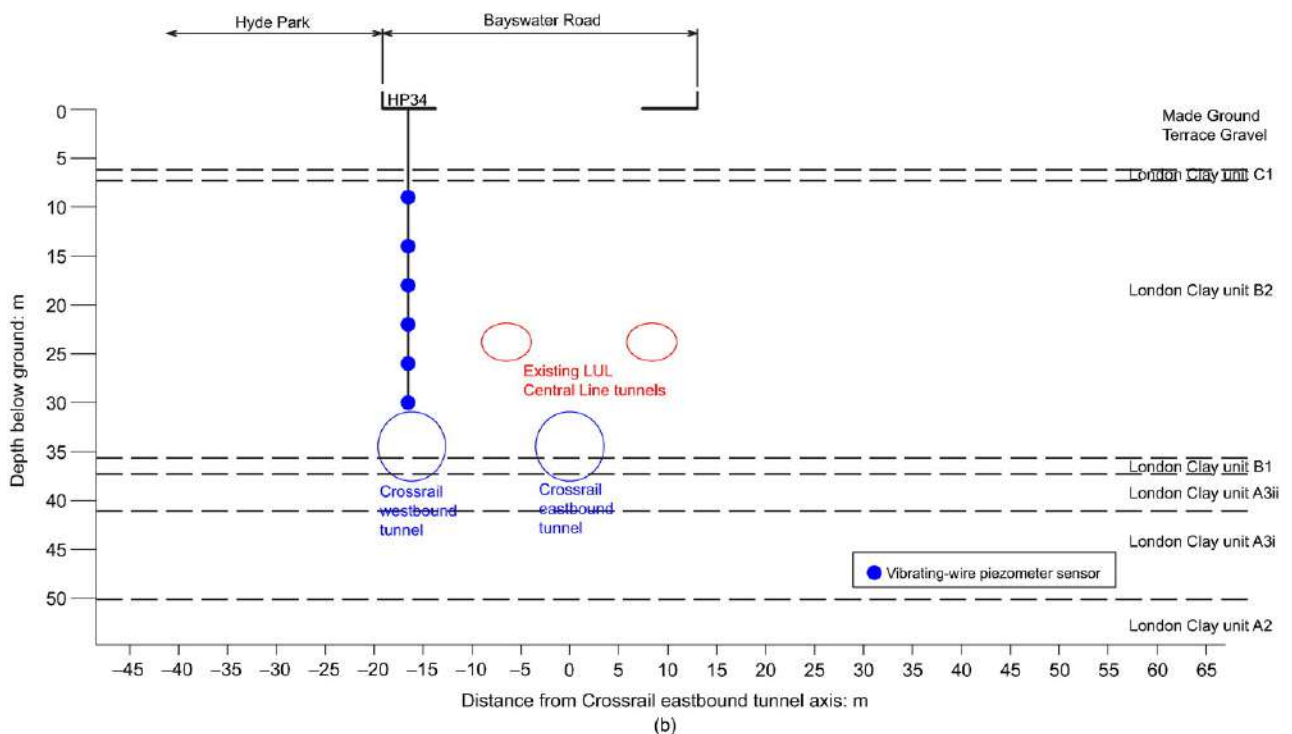
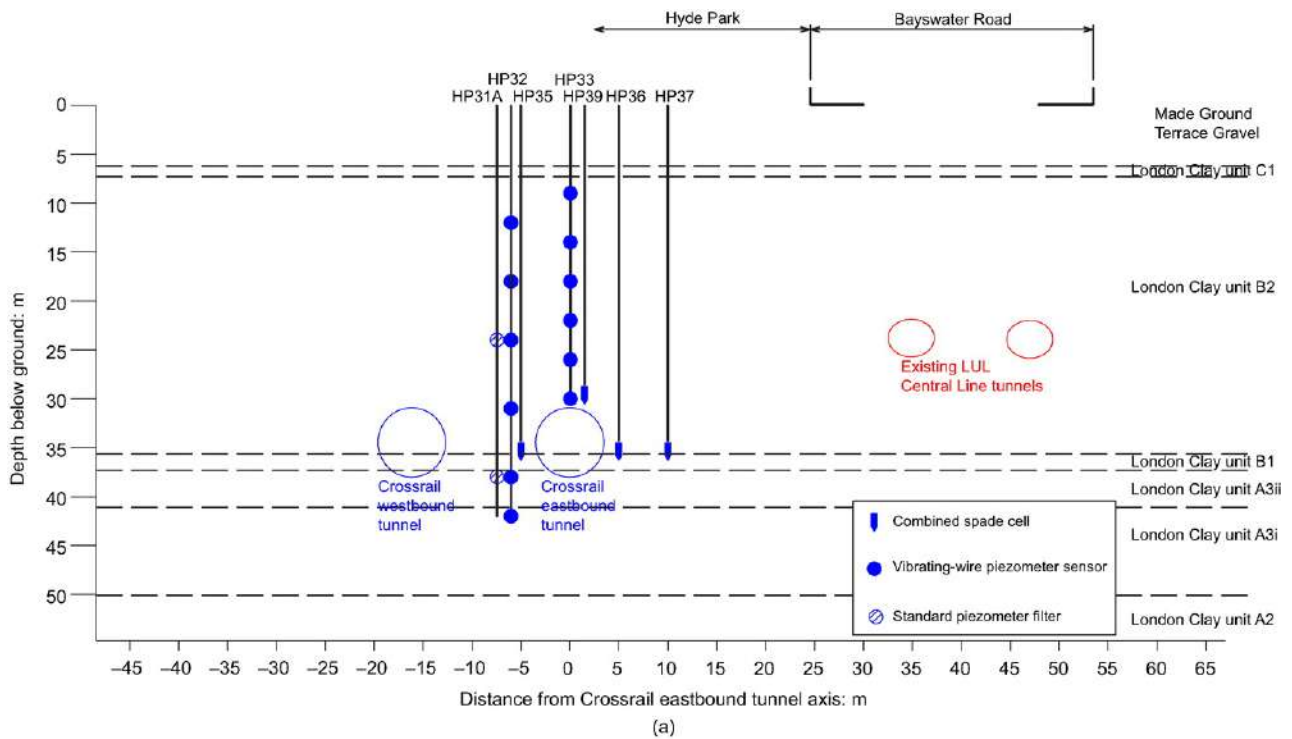


Fig. 2. (a) Cross-section of main array of piezometers and spade cells (section A-A). (b) Cross-section of piezometers in Bayswater Road (section B-B)

The spade cell type installed at the site (also manufactured by Soil Instruments Ltd) consists of a flat, rectangular (with

a point at one end), spade-shaped oil chamber (formed by two 100 mm wide steel plates) connected to a VW pressure

transducer with a measurement range of 2000 kPa. This measures total stresses acting on the pressure cell in the direction perpendicular to the spade surface. In-built at the top of one side of the spade is a porous filter, which is connected to a separate VW pressure transducer, so that the pore water pressure is measured independently at the same time. Each spade cell was installed by first drilling a borehole to a pre-determined depth (about 1 m above the target instrument depth). The spade cell, attached to a string of rods, was then lowered to the borehole base, before being pushed vertically to the target depth. The orientation of each spade cell was carefully adjusted so that the flat spade was parallel to the alignment of the eastbound Crossrail tunnel so as to make measurements of stress changes in the transverse direction. [Wan & Standing \(2014b\)](#) describe the installation procedure.

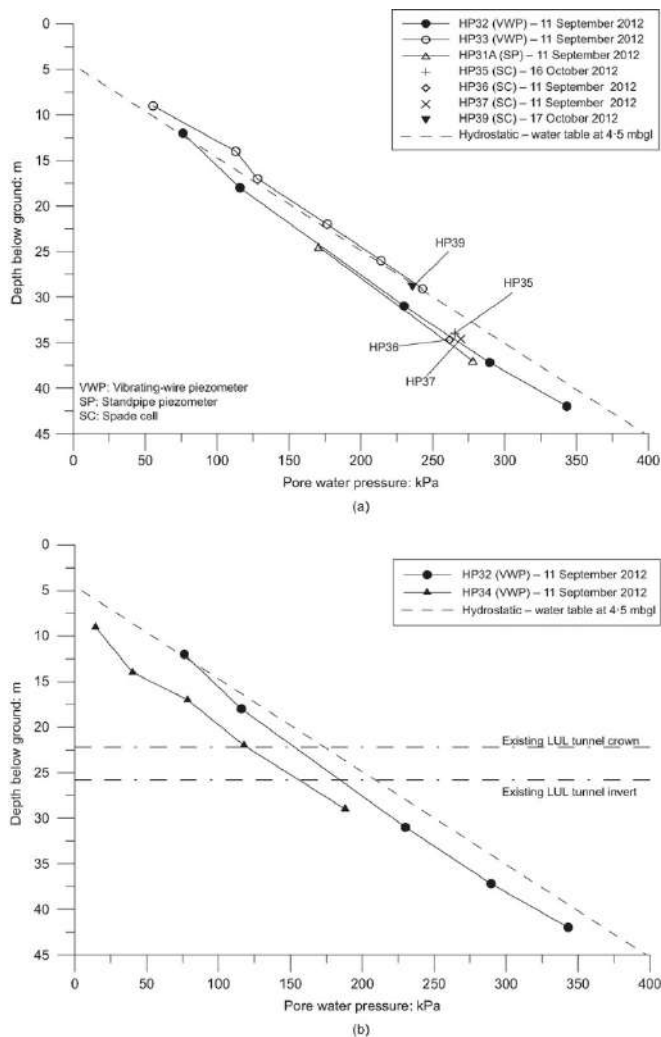


Fig. 3. Measured steady-state pore water pressures (after-Wan & Standing, 2014b): (a) in 'greenfield' ground by standpipe piezometer (HP31A), VW piezometers (HP32 and HP33) and spade cells (HP35, HP36, HP37 and HP39); (b) in the vicinity of the existing LUL running tunnels by VW piezometers (HP34) (HP32 also shown for reference)

From the literature it is well established that pushed-in spade cells provide overestimates of ground stresses. [Tedd & Charles \(1981\)](#) investigated the measurement of in situ stress in London Clay by comparing horizontal stress measurements using spade cells with other in situ stress measuring instruments such as self-boring pressuremeters, whereas [Tedd & Charles \(1983\)](#) and [Ryley & Carder \(1995\)](#) compared

the in situ overburden pressure with the vertical stress measured by spade cells installed horizontally, and found that the measured values need to be corrected by about half the undrained shear strength. [Tedd et al. \(1989\)](#) reviewed spade cell measurements from a number of sites in soft and stiff clays and found that generally the spade cells tend to over-read the actual total horizontal stress due to the complex local stresses on the spade surface induced by the installation pushing process. The over-read error based on all the above studies depends on the soil stiffness and can range widely from 0.3 to 2.0 times the undrained shear strength. It should be noted that the wide range of over-read factors determined from these studies can be attributed to a combination of errors associated with the 'true readings' that the spade cell measurements were compared with, and variability in the measurement of the undrained shear strength induced by different testing methods and sample dimensions. More recently, [Richards et al. \(2007\)](#) investigated the total vertical stress measured by horizontally installed spade cells under a box excavation in stiff Atherfield Clay, and reported that the over-read was about 0.35 times the undrained shear strength (determined from unconsolidated undrained tests on 100 mm dia. samples and standard penetration test measurements) compared with the actual overburden pressure. They also found that the spade cells under-read the change (reduction) of vertical stress upon the removal of overburden due to excavation, but concluded that the discrepancy was a result of shear stress mobilised between the ground and the perimeter wall (wall adhesion) resisting the ground heave, rather than a result of over-compliance of the spade cell (i.e. it being insufficiently stiff compared with the ground).

In general, the spade cell would either over-read or under-read the change of total stress depending on the relative cell/soil stiffness. For the type of spade cell used at the Hyde Park site, the cell stiffness is high compared even with the small strain stiffness of London Clay. Therefore the spade cells would tend to over-read the horizontal stress changes induced by the tunnel construction, although it is difficult to quantify the over-read accurately.

Having discussed the various limitations of using spade cells, it is also worth commenting that when monitoring the three-dimensional ground response to EPBM tunnelling, there is little ambiguity in measuring displacements, as individual devices (e.g. extensometers and inclinometers) are specifically designed to measure respective vertical and horizontal components. However, when measuring pore water pressure and total stress changes, a greater appreciation of the three-dimensional effects is needed to interpret the field data correctly.

#### Measured EPBM operation variables

The operation variables of the two EPBMs were recorded as they advanced. [Wan et al. \(2017a\)](#); Fig. 23) present the recorded face pressure, tail grout pressure and tail grout volume for both TBM1 and TBM2 (west- and eastbound construction, respectively) relating to when they were driven over about a 1 km distance beneath Hyde Park. In terms of rolling averages over ten lining rings, face pressures were maintained at about 200 kPa for both TBM1 and TBM2, while tail grout pressures were slightly more variable but broadly maintained at about 100 kPa for TBM1 and 200 kPa for TBM2. The in situ total overburden pressure at tunnel axis level under Hyde Park is about 650 kPa.

The EPBM face pressures and tail grout pressures are examined in more detail for when the TBM drives were in close proximity of where the piezometers were installed. [Figs 4\(a\)](#) and [4\(b\)](#) show the EPBM pressures, based on rolling averages over three rings, within  $\pm 30$  m of the piezometers and spade

cells for TBM1 and TBM2, respectively. As both TBMs approached and passed the instruments, the face pressures were fairly consistent, ranging mostly between about 180 kPa and 220 kPa, whereas the tail grout pressures were more variable, ranging from 40 kPa to 240 kPa. As the tail grout pressures relate to the rear of the TBMs, for clarity, schematic

representations of the TBMs in relation to the monitoring point are provided in Fig. 4. When comparing EPBM pressures with measured pore water pressure and total stress changes, the EPBM values shown in Table 1 are adopted for each instrument.

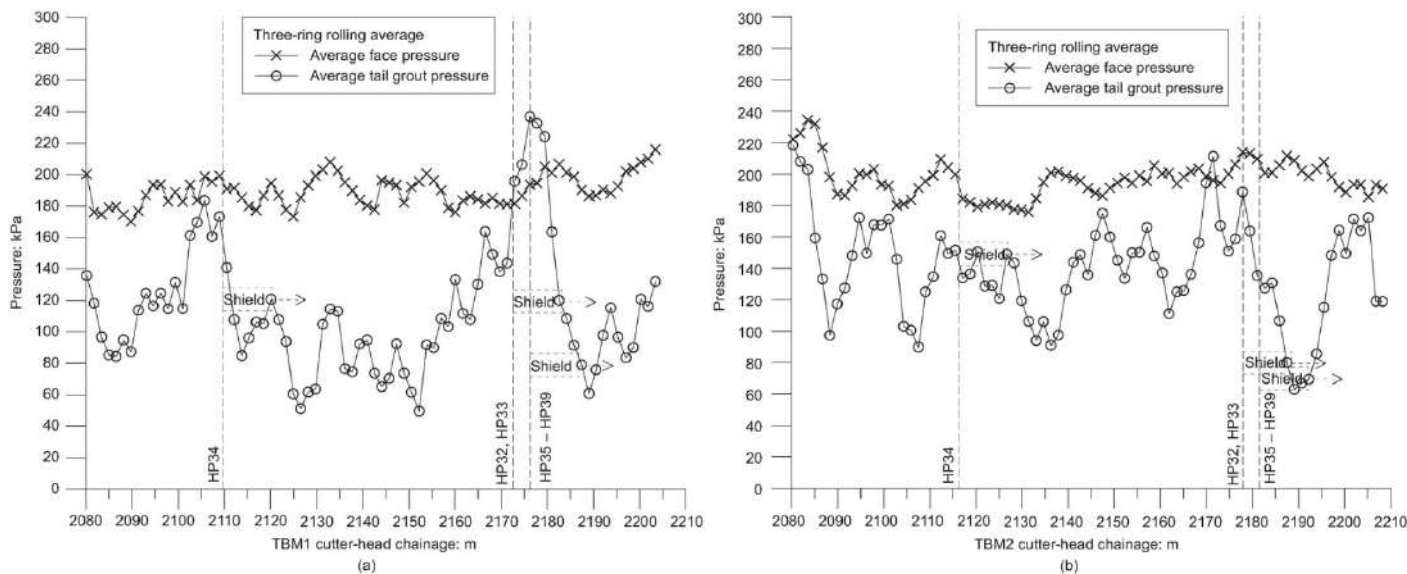


Fig. 4. Measured average face pressure and tail grout pressure of: (a) TBM1; (b) TBM2

Table 1. Average face pressure and tail grout pressure when the cutter-head or shield tail of both TBMs passed the instrument boreholes

Instrument borehole	TBM1		TBM2	
	Face pressure: kPa	Tail grout pressure: kPa	Face pressure: kPa	Tail grout pressure: kPa
HP34	190	120	200	150
HP32, HP33	180	120	210	80
HP35, HP36, HP37, HP39	195	80	200	70

## MONITORING RESULTS

The pore water pressure and total stress monitoring data were divided into the same five periods used in the companion papers.

- Period 1 – pre-construction (12 October 2011 to 19 November 2012).
- Period 2 – construction of the westbound tunnel by TBM1 (19 November 2012 to 30 November 2012).
- Period 3 – interim phase before TBM2 arrived (30 November 2012 to 3 February 2013).
- Period 4 – construction of the eastbound tunnel by TBM2 (3 February 2013 to 12 February 2013).
- Period 5 – long-term monitoring (12 February 2013 onwards).

The sign conventions for presentation of the monitoring results are as follows.

- (a)  $x_f$  is the longitudinal horizontal distance between the cutter-head and the monitoring point/line in question.  $(-)$  $x_f$  means the cutter-head is approaching the monitoring

point/line while  $(+)$  $x_f$  means the cutter-head is progressing beyond the monitoring point/line.

- (b) Positive  $(+)$  $y$  means the transverse horizontal distance from the tunnel axis to the left-hand side when looking in the direction of tunnel advancement.

- (c) Negative  $(-)$  $z$  means the downwards vertical distance from the ground surface, but depth (mbgl) is always expressed as positive values.

### Initial steady-state pressures

Post-installation and steady-state pore water pressure and total horizontal stress measurements before the tunnel construction (period 1) are discussed by Wan & Standing (2014b) and Wan (2014), while this paper concentrates on the short-term responses observed during periods 2 and 4. The profiles of steady-state pore water pressure before the arrival of TBM1 as reported in Wan & Standing (2014b) are shown in Fig. 3. Note that before the tunnel construction, all piezometers were expected to measure greenfield ground pore water pressures except for HP34, which is located 5 m from the existing Central Line westbound tunnel. The greenfield measurements from HP32 (Fig. 3(a)) indicate a slightly under-drained steady-state piezometric profile within the LCF, while it is evident from the measurements from HP34

(Fig. 3(b)) that the steady-state pore water pressure near the existing Central Line tunnels is reduced, indicating that these tunnels, with cast-iron segmental linings, drain the surrounding ground. It should be noted that the profile for HP33

would also be expected to register slight under-drainage, but is close to hydrostatic because of suspected connectivity between the lower devices, as explained by [Wan & Standing \(2014b\)](#).

Table 2. Steady-state pore water pressures and total horizontal stress (uncorrected by over-read factor) measured by combined spade cells, and estimated  $K_0$  before tunnel construction

Instrument borehole	Depth of spade mid-point: mbgl	Pore water pressure: kPa	Total horizontal stress: kPa	Estimated at-rest lateral earth pressure coefficient, $K_0$
HP35	34.3	263	267	N/A
HP36	35.0	266	1077	2.1
HP37	34.9	273	1201	2.4
HP39	29.2	234	838	1.9

N/A, not applicable.

The total horizontal stresses measured by the spade cells (without correction of any factor of undrained shear strength) before the tunnel construction are given in [Table 2](#) (note that the undrained shear strength determined from unconsolidated undrained triaxial tests on 100 mm dia. samples from boreholes in Hyde Park ranges from 150 kPa to 400 kPa at the level of the Crossrail tunnels (see Fig. 9 in [Wan & Standing \(2014a\)](#)). Using these uncorrected measured total horizontal stresses in conjunction with the known overburden stress and the measured pore water pressure at the depth of the spade cells, the at-rest lateral earth pressure coefficients ( $K_0$ ) can be deduced and are also presented in [Table 2](#). With the exception of the spade cell HP35, which measured unrealistically low total horizontal stress, the derived in situ  $K_0$  values at the depths of spade cells HP36, HP37 and HP39 fall within a range from 1.9 to 2.4. Taking into account the likely over-read of the in situ stresses by spade cells, it is considered that these  $K_0$  values are reasonable. Nearby, at Paddington,  $K_0$  values of up to about 1.7 derived from self-boring pressuremeter measurements and independent suction measurements of undisturbed samples near the depth of the Crossrail tunnel axis level – that is, near the base of London Clay unit B ([GCG, 2009](#)) – corroborate the measured initial values of total horizontal stress from the spade cells. Typically, the design  $K_0$  value of London Clay in central London, considering the historical erosion of top clays and subsequent reloading of superficial deposit, ranges from 1.0 to 1.5 ([Burland et al., 1979](#)).

#### Measurement frequency during tunnel construction (passages of TBM1 and TBM2)

For the multi-level VW piezometers and combined spade cells, during periods 2 and 4, hourly readings were taken and recorded automatically by data-loggers within each borehole headworks, except spade cells HP36 and HP37 where readings were taken manually using a hand-held VW readout unit three to four times a day owing to faulty data-loggers.

In the next sections the measurement results are presented in terms of either time or the distance,  $x_r$ , of the EPBM cutter-head relative to the monitoring line. The progression of both TBM1 and TBM2 with time is given by [Wan et al. \(2017a: Fig. 6\)](#).

#### MEASURED IMMEDIATE RESPONSES TO THE WEST-BOUND TUNNEL CONSTRUCTION (TBM1, PERIOD 2)

In this section the responses of the three multi-level piezometers are discussed individually (for period 2), starting with HP32 and HP33, which are located in ground where a more greenfield response would be expected. HP34, located close to the existing Central Line tunnels is covered next. The com-

bined total stress transducer–piezometer spade cells (HP35, HP36, HP37 and HP39), clustered around the eastbound tunnel, are then covered collectively.

#### Response of HP32 piezometers (TBM1, period 2)

Changes in pore water pressure,  $\Delta u$ , measured by the VW piezometer sensors in HP32 as TBM1 passed are presented in [Fig. 5\(a\)](#). In plan HP32 is about 10.8 m from the TBM1 centre-line, or one tunnel diameter from the extrados of the excavation. No measurement results are shown for the sensor at  $z = -24.5$  m as it was faulty. Pore water pressures started to change at all elevations when  $x_r = -30$  m. At about 25 m in front of the HP32 piezometers ( $x_r = -25$  m), TBM1 stopped advancing for about 31 h because of problems with the spoil muck-away system. During this time the pore water pressures measured within HP32 over the depth of the TBM ( $-31 \text{ m} < z < -42 \text{ m}$ ) fluctuated by a small degree: within about  $\pm 3$  kPa. This incident did not cause significant settlement measured by the surface settlement points ([Wan et al., 2017a: Fig. 8\(a\)](#)) or subsurface rod extensometers ([Wan et al., 2017b: Fig. 3](#)).

The pore water pressures at the measurement depths, except that furthest from the TBM at  $z = -12$  m, increased as the TBM cutter-head approached, peaking when it was about 5 m beyond the instruments ( $x_r = 5$  m). A maximum pore water pressure change of about +22 kPa was measured at the elevations near TBM1 crown and invert levels ( $z = -31.0$  m and  $z = -37.2$  m) which are equidistant from the axis of TBM1. The fact that these piezometers measured pore water pressure increases of a similar magnitude suggests that they are measuring an essentially undrained response to the TBM cutter-head approaching, despite the fact that the lower device is just within the more permeable A3ii sub-division of the LCF (see [Fig. 2](#)). Since the TBM face pressure (about 180 kPa on average) was lower than the overburden pressure at the tunnel axis level (about 650 kPa), it is believed that the pore water pressure increase in front of the TBM cutter-head was caused by ground arching in front of and around the TBM shield face (discussed in the section entitled 'Mechanisms of EPBM tunnelling-induced pore water pressure changes and ground arching').

As the TBM advanced and passed beyond the instruments, the pore water pressures at all elevations decreased as a result of the predominantly undrained unloading caused by the excavation until the TBM1 cutter-head was at a distance of about  $x_r = 25$  m. The magnitude of the final change of the pore water pressure depends on the balance between the loading and unloading effects, the distance from the TBM, and also the permeability of the London Clay at the point of measurement. The undrained shearing of the overconsolidated clay would also generate additional negative excess pore water

pressure. It appears that the shallowest sensor at  $z = -12$  m was too far from TBM1 to be affected by the effect of the approaching cutter-head, but measured a slight decrease in pore water pressure due to the effect of ground unloading. The TBM1 tail leaving the instruments does not seem to have any significant effect on the pore water pressure (near  $x_f = 10$  m) in HP32, although a very minor effect is noticed for the two sensors near the TBM crown and invert levels. By the time TBM1 is 60 m from HP32, all sensors have essentially stabilised, with the two shallowest ones being within  $\pm 5$  kPa of their original values and the others with net negative changes (the largest being  $\Delta u = -16$  kPa at  $z = -42.0$  m).

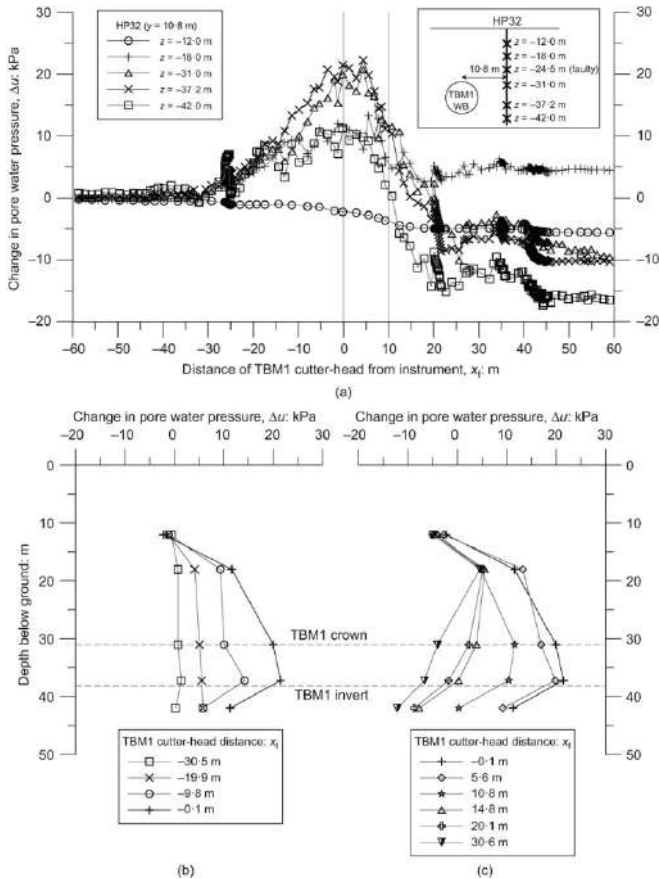


Fig. 5. Change in pore water pressure measured in piezometer HP32 in response to westbound construction (period 2): (a) variation with TBM1 cutter-head distance; (b) depth profiles when the TBM1 cutter-head was approaching the instrument; (c) depth profile when TBM1 cutter-head was leaving the instrument

Before stabilising, there are two points in time (at  $x_f$  distances of about +20 m and +40 m) when the sensors closer to the TBM appear to indicate marked, but small ( $< 5$  kPa), reductions in pore water pressure, the magnitudes of which decrease with increasing distance of the TBM from the sensors. The data points, which represent hourly readings, are closely clustered at these  $x_f$  distances and so coincide with times at which the TBM slowed down or was not advancing. The reason for the reductions is not known. Similar responses are also observed when the TBM slows down in some of the later plots.

Many of the observations described above are evident from vertical profiles of pore water pressure changes measured in HP32, which are plotted separately as TBM1 was approaching (Fig. 5(b)) and leaving HP32 (Fig. 5(c)). It is clear from these figures that the increase in pore water pressure in response

to the TBM1 face approaching and then the subsequent reduction due to ground unloading was greatest at the TBM horizons.

### Response of HP33 piezometers (TBM1, period 2)

Changes in pore water pressure measured by the VW piezometers in HP33 during period 2 are presented in terms of cutter-head distance in Fig. 6(a). HP33 is at a greater distance away from TBM1 than HP32 (about 16.0 m in plan from its centre-line) and therefore the overall response was of smaller magnitude. As with HP32, pore water pressures also started to change when  $x_f = -30$  m. The effect of the TBM1 stopping at  $x_f = -25$  m was not as obvious as measured in HP32 as HP33 was further from the tunnel. As the TBM1 cutter-head approached and passed beyond HP33, pore water pressure at the deeper four elevations gradually increased with a maximum  $\Delta u$  of about +15 kPa measured at  $z = -29.0$  m near the TBM1 crown level. Only small changes ( $\Delta u < 10$  kPa) were measured at the two shallowest sensor elevations ( $\Delta u \sim 0$ , at  $z = -9$  m). There was no discernible pore water pressure response above the TBM1 crown level to the ground unloading (i.e. pressure drop), as the shield tail passed HP33 (around  $x_f = 10$  m), except a small reduction at  $z = -14$  m. The response of the piezometer at this depth is slightly erratic at earlier TBM positions (e.g.  $x_f = -18$  m) and so the output from it could be erroneous, especially given the piezometer responses above and below it (at  $z = -9$  and  $-17$  m). Therefore, overall the effect of stress relief or shearing due to excavation was not registered by the piezometers within HP33.

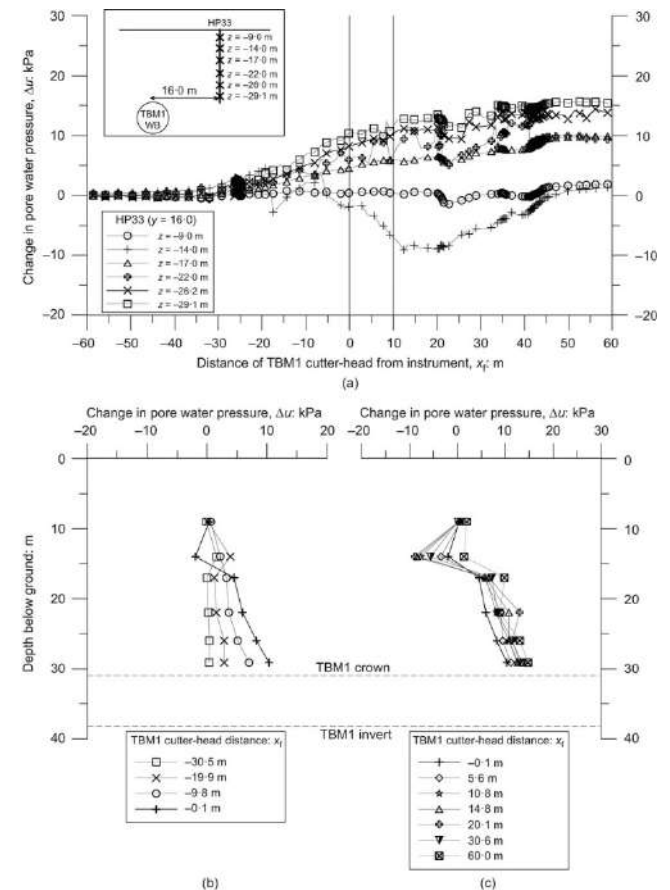


Fig. 6. Change in pore water pressure measured in piezometer HP33 in response to westbound construction (period 2): (a) variation with TBM1 cutter-head distance; (b) depth profiles when the TBM1 cutter-head was approaching the instrument; (c) depth profile when TBM1 cutter-head was leaving the instrument

Similar to the observation for HP32 (Fig. 5(a)), there were marked reductions in pore water pressure measured by the HP33 sensors at  $x_r = +20$  m, when the TBM advance slowed down, but their magnitudes are even smaller than those measured in HP32.

Profiles of  $\Delta u$  with depth when TBM1 was approaching and passing beyond HP33 are shown in Figs 6(b) and 6(c), respectively, and reflect many of the observations made above (especially regarding the piezometer at  $z = -14$  m: if the data from this device were omitted the profiles would be far more uniform). As discussed in Wan & Standing (2014b), the lowest three piezometers within HP33 were found during the pre-construction monitoring to be interconnected after installation. Despite this, independent immediate pore water pressure changes still seem to have been measured reliably by these three lowest sensors in response to the rapid loading and unloading during tunnel construction, with the pressure increase decreasing with distance from the tunnel crown.

### Response of HP34 piezometers (TBM1, period 2)

Multilevel piezometer borehole HP34 is 5 m in plan from the extrados of the westbound Central Line tunnel and was located directly above TBM1 when it passed, with the deepest sensor at  $z = -29.0$  m, just 2 m above its crown. Consequently the measured pore water pressures might have been expected to be more pronounced as TBM1 approached and passed.

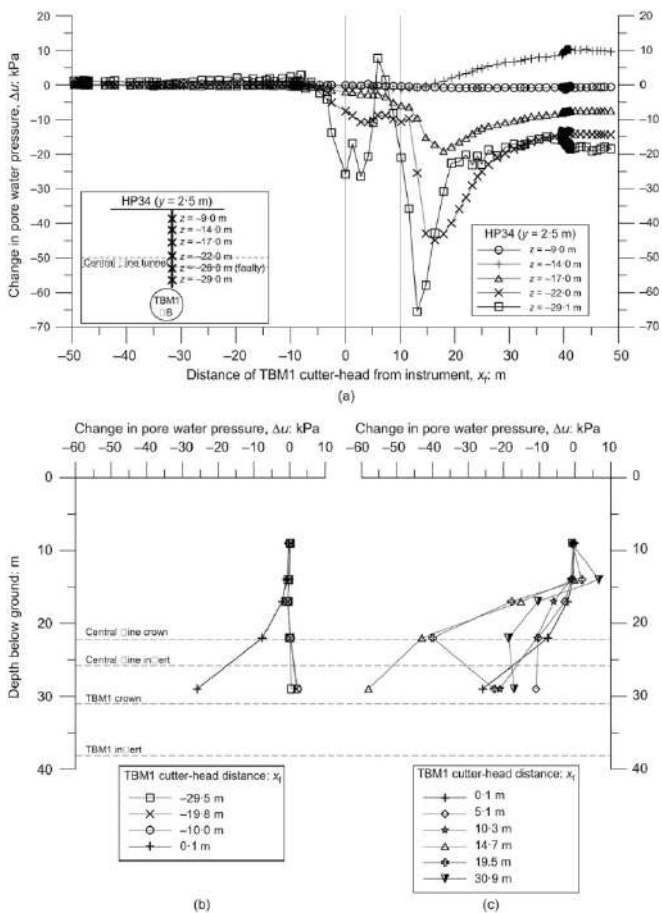


Fig. 7. Change in pore water pressure measured in piezometer HP34 in response to westbound construction (period 2): (a) variation with TBM1 cutter-head distance; (b) depth profiles when the TBM1 cutter-head was approaching the instrument; (c) depth profile when TBM1 cutter-head was leaving the instrument

It can be seen from the measured values of  $\Delta u$  presented in Fig. 7(a) that this was not so (results from the piezometer at  $z = -26$  m are not shown as it was faulty). Increases in pore water pressure were less than 5 kPa as TBM1 approached HP34, compared with an increase of up to 22 kPa and 11 kPa measured at HP32 and HP33, respectively, which were more than 10 m horizontally from the TBM1 centre-line. The reduced increase in  $\Delta u$  probably occurs because of the close proximity of the adjacent existing Central Line tunnels, which would have affected the ground loading/unloading pattern and the development of any ground arching in front of the advancing TBM cutter-head.

Pore water pressures started to decrease when the cutter-head was about 7 m, or about one tunnel diameter, in front of HP34 ( $x_r = -7$  m). The greatest recorded change was at  $z = -29$  m, above which values decreased with increasing elevation above the TBM1 crown. Pressures continued to decrease until about  $x_r = 4$  m as negative excess pore water pressures were generated as a result of unloading around the front section of the shield body (i.e. soil closing into the annular void created by the tapering shield) and possibly also shearing of the overconsolidated clay. Subsequently, at elevations closer to the TBM1 crown (i.e.  $z = -22$  m and  $-29$  m), pore water pressures rebounded by up to 35 kPa. This could be a consequence of the tail grout pressure compressing the ground (even though the main effect of the grouting would be expected directly behind the rear of the shield) and correlates exactly with what was observed from the response of the extensometers directly above TBM1 as reported by Wan et al. (2017b: Fig. 3(b)). (Note that the comparison made relates to extensometer HP20, which is about 38 m from HP34. However, the response of extensometer HP26, directly adjacent to HP34, was very similar but with a less marked rebound (this response was not presented in the Wan et al. (2017b) paper but was in the thesis by Wan (2014)).) Ground heave from tail grouting occurred at about  $x_r = 7$  m, in advance of the back of the shield passing beneath the measuring point, followed by a rapid settlement. Another explanation for this increase in  $\Delta u$  (rebound) before the back of the shield passes beneath HP34 can again be provided by a mechanism of ground arching. Ground arches would form around locations where ground losses are greatest and the ground has softened or 'yielded' (i.e. at the shield tail where tail void closure starts to occur before the grouting comes into effect). The ground arching would compress the ground in front of and behind the shield tail, leading to increases in pore water pressure (discussed further in the section entitled 'Mechanisms of EPBM tunnelling-induced pore water pressure changes and ground arching').

Similarly, in terms of pore water pressure changes, following the rebound,  $\Delta u$  values dropped rapidly at the deeper elevations as the rear of TBM1 passed beyond HP34 (Fig. 7(a) from  $x_r = 7$  m onwards). This reduction in  $\Delta u$  occurred as the shield was advanced and the ground lost the support of the shield body, leading to further ground loss into the gap between the tail-skin and the extrados of the newly erected tunnel linings (tail void closure). A maximum reduction of pore water pressure of about  $-75$  kPa was measured at  $z = -29$  m when  $x_r = 13$  m. A similar response in terms of displacement was observed (Wan et al., 2017b: Fig. 3(b)). It is evident that, for the ground near the shield tail ( $x_r = 10$  m) the effect of tail void closure (stress relief) significantly outweighs the effect of tail grout pressure (compressing the ground). Soon afterwards the pore water pressures began to recover as the newly erected tunnel linings, in conjunction with tail grout setting and becoming stiffer, started to support the annulus between their extrados and the ground and also because of the development of ground arching across the rear of the shield. For the three operational sensors above the TBM1

crown ( $-29\text{ m} < z < -17\text{ m}$ ), the final pore water pressures were smaller than those prior to the construction.

Profiles of pore water pressure changes with depth for the periods when TBM1 approached and passed beyond HP34 are shown in [Figs 7\(b\)](#) and [7\(c\)](#).

### Response of spade cells HP35, HP36, HP37 and HP39 (TBM1, period 2)

As can be seen from [Fig. 1](#), the spade cells are all very close to the eastbound tunnel alignment (therefore at some distance away from TBM1). Changes in pore water pressures,  $\Delta u$ , and total horizontal stresses,  $\Delta \sigma_h$ , measured by the spade cells in response to the westbound construction are shown in [Fig. 8](#). Spade cell HP39 was located at the same  $y$ - $z$  position as the deepest piezometer of HP33: its pore water pressure response, as shown in [Fig. 8\(a\)](#), has a similar pattern, with an increase in pressure (cf. [Fig. 6\(a\)](#)), but of slightly greater magnitude than the deepest piezometer in HP33 as TBM1 progressed. A potential reason for the differences in magnitude is that the piezometer within the spade cell responds more simultaneously with total stress changes as it is in direct contact with the ground (from pushing in the device) compared with the multi-level piezometer installed within a grout column. The other three spade cells HP35, HP36 and HP37, located at the elevation of the TBM axis, also exhibited similar pore water pressure responses but of smaller magnitude. Spade cell HP35, closest to TBM1 (11 m from its centre-line or about one diameter from the tunnel extrados), measured a slight drop of pore water pressure at  $x_f \approx 20\text{ m}$ , compared with the other three devices which showed a small increase.

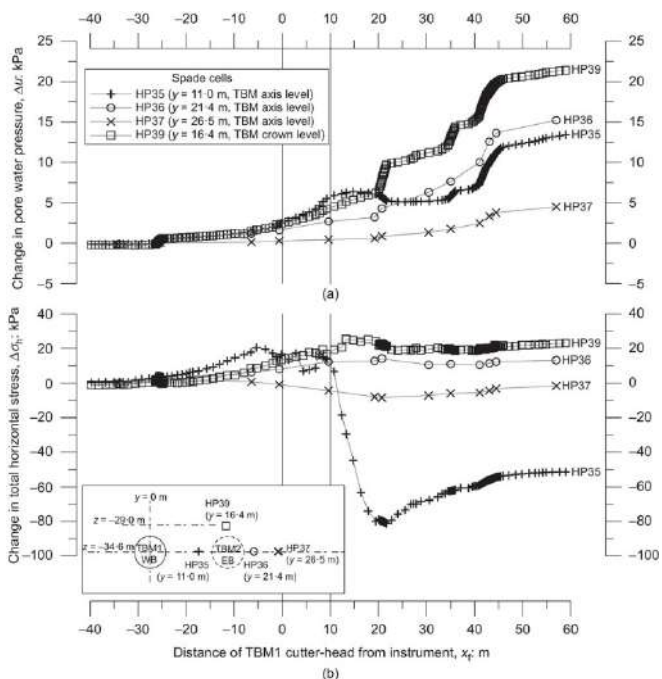


Fig. 8. Change in (a) pore water pressure and (b) total horizontal stress measured in spade cells HP35, HP36, HP37 and HP39 in response to westbound construction (period 2)

Total horizontal stress changes,  $\Delta \sigma_h$ , transverse to the axis of the tunnel are shown in [Fig. 8\(b\)](#). Those measured by HP35 were the largest in magnitude, it being the closest spade cell to TBM1 (although still 11 m from its axis). At this location, the total stress initially increased by 20 kPa in response to the approaching cutter-head (probably associated with ground arching in front of the cutter-head). The unloading

effect in the vicinity of the rear of the shield as it passed is evident as a rapid, large drop in total stress (for  $x_f > 10\text{ m}$ ). A maximum decrease of about  $-80\text{ kPa}$  was measured at  $x_f = 20\text{ m}$ , before  $\sigma_h$  started recovering. The net total stress reduction was measured to be about  $-50\text{ kPa}$ , indicating the overall effect of the tunnel excavation and the newly erected tunnel lining supporting the ground. Additionally, as HP35 is located within the very silty B1 sub-division, some pore water pressure dissipation might occur in the short term.

At the other spade cells (HP36, HP37 and HP39) further away from TBM1, initial increases in total stresses were smaller (up to  $+10\text{ kPa}$ ) as TBM1 advanced and passed, followed by negligible subsequent drops and rises after the initial increases (less than  $\pm 5\text{ kPa}$ ) compared with the response observed for HP35.

### Further interpretation

It is instructive to compare the total stress change responses with corresponding displacements measured using rod extensometers (vertical) and inclinometers (horizontal) as presented and discussed by [Wan et al. \(2017b\)](#). In terms of vertical displacements at axis level, the maximum magnitude was less than 4 mm downwards at extensometer HP22 ([Wan et al., 2017b](#): Fig. 4), which is closer than spade cell HP35 from the TBM1 axis (8.1 m compared to 11.0 m), although this sense of displacement might not have much influence on the spade cells orientated to measure horizontal stresses. In terms of horizontal displacements, no face pressure-induced outward movement was observed, even close to the tunnel (see details given of horizontal displacements at closest inclinometer borehole HP6, as shown in Fig. 10(a) in the paper by [Wan et al. \(2017b\)](#)) while  $\Delta \sigma_h$  increased (by up to about 20 kPa) in HP35 as TBM1 approached the instrument. The subsequent reduction in  $\Delta \sigma_h$  within HP35 correlates with the horizontal displacements in towards the tunnel observed from inclinometer HP7 (at the same, closer, offset as extensometer HP22) as TBM1 progressed beyond it ([Wan et al., 2017b](#): Fig. 11). At this offset, no reversal of displacements was observed from tail grouting as was observed for inclinometer HP6 ([Wan et al., 2017b](#): Fig. 10(b)). Qualitatively the measured displacements and total horizontal stress changes correlate with each other.

### MEASURED IMMEDIATE RESPONSE TO EASTBOUND TUNNEL CONSTRUCTION (TBM2, PERIOD 4)

Piezometer and spade cell measurements are presented and discussed in this section in the same order as previously. Generally responses were much more marked for the eastbound tunnel construction (TBM2) as the devices (except HP34) were much closer to this excavation and trends in changes were broadly similar.

### Response of HP32 piezometers (TBM2, period 4)

HP32 lies very close to the tunnel construction, being about 1.5 m (less than half of a tunnel radius) horizontally from the TBM2 extrados, resulting in a much greater pore water pressure response than that from the westbound tunnel construction. Changes in  $\Delta u$  measured by the five operational piezometers in HP32 as TBM2 passed are shown in [Fig. 9\(a\)](#), where it can be seen that  $\Delta u$  increased at all elevations, except the shallowest one, when TBM2 was at  $x_f = -40\text{ m}$ , rising rapidly by  $x_f = -15\text{ m}$ . Peak increases were measured within  $-10\text{ m} < x_f < -3\text{ m}$ , depending on the individual piezometer elevations. A maximum change of about  $+50\text{ kPa}$  was measured at elevations near the TBM2 crown and invert levels ( $z = -31.0\text{ m}$  and  $-37.2\text{ m}$ ) in response to the approaching TBM2 cutter-head and the development of ground arching. Pore water pressures then dropped rapidly by up to 130 kPa

near  $x_f=0$  m, from the unloading and shearing associated with the excavation and advance of the shield. These  $\Delta u$  values suggest that conditions were essentially undrained. The effect of tail grouting (average pressure of about 80 kPa) and the development of ground arching is evident from pore water pressures starting to recover between  $5\text{ m} < x_f < 10\text{ m}$  with rebounds ranging from 30 kPa to 50 kPa at elevations close to TBM2 (as noted for TBM1, these increases occur well in advance of the tail skin reaching the monitoring position). This correlates very well with the ground being temporarily pushed outwards by the tail grout in advance of the TBM2 tail skin as measured by inclinometer HP9, which was at a similar offset distance to the TBM2 axis but on the other side (Wan et al., 2017b: Figs 12 and 13).

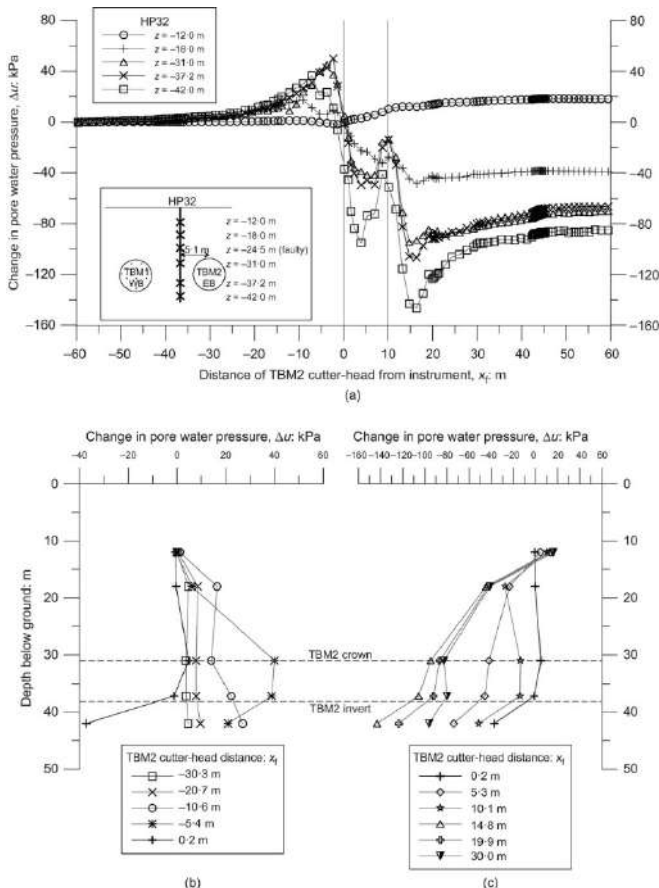


Fig. 9. Change in pore water pressure measured in piezometer HP32 in response to eastbound construction (period 4): (a) variation with TBM2 cutter-head distance; (b) depth profiles when the TBM2 cutter-head was approaching the instrument; (c) depth profile when TBM2 cutter-head was leaving the instrument

As the shield tail passed beyond HP32,  $x_f > 10$  m, there was a second rapid reduction as a result of further unloading (tail void closure). The maximum net reduction of pore water pressure was about  $-150$  kPa measured below the tunnel invert at  $z = -42$  m when  $x_f \approx 15$  m. Pore water pressures then started to recover by different degrees from the tail grout setting and becoming stiffer as TBM2 advanced further.

The depth profiles of the change in pore water pressures measured in HP32 as TBM2 was approaching and leaving are shown in Figs 9(b) and 9(c), respectively, and reflect the trends described above. Being nearest to the TBM location, the sensors at  $z = -31$  m and  $-37.2$  m measured the greatest pore water pressure increase when the TBM cutter-head was approaching (when  $x_f = -5.4$  m). As TBM2 passed beyond HP32, the piezometer at  $z = -42$  m, being the deepest one,

experienced the largest unloading as the ground above it was excavated and hence measured the greatest pore water pressure reduction.

**Response of HP33 piezometers (TBM2, period 4)**

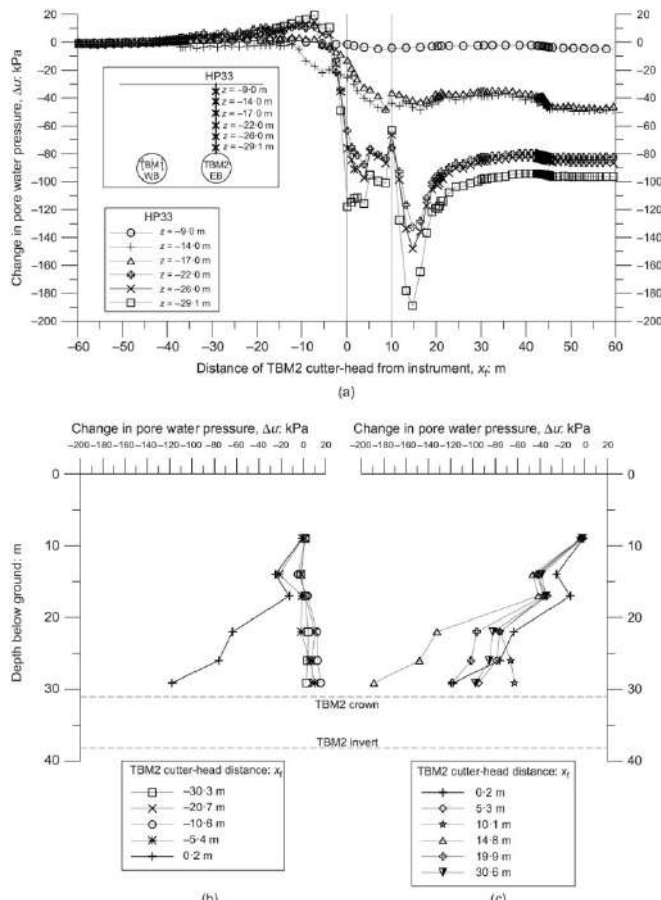


Fig. 10. Change in pore water pressure measured in piezometer HP33 in response to eastbound construction (period 4): (a) variation with TBM2 cutter-head distance; (b) depth profiles when the TBM2 cutter-head was approaching the instrument; (c) depth profile when TBM2 cutter-head was leaving the instrument

The  $\Delta u$  values measured by the piezometers in HP33 as TBM2 passed beneath them are presented in Fig. 10(a). The measured responses to the eastbound construction show a very similar pattern to those of HP34 in response to the westbound construction (see Fig. 7(a)), but are generally of larger magnitude. In particular, the pressure increase measured by HP33 ahead of the cutter-head was more pronounced, probably because ground arching in front of the cutter-head could develop freely without any interference from the existing Central Line tunnels. Pore water pressures increased (up to  $+20$  kPa) as the TBM2 cutter-head approached, followed by: a rapid drop of pore water pressure near  $x_f = 0$  m; subsequent rebound between  $10\text{ m} < x_f < 15\text{ m}$ ; and subsequent partial recovery. The greatest net reduction of pore water pressure was about  $-190$  kPa at  $z = -29$  m when  $x_f = 15$  m. Profiles of  $\Delta u$  with depth as TBM2 was approaching and leaving are presented in Figs 10(b) and 10(c), respectively. The deepest piezometer at  $z = -29$  m, about 2 m above the TBM crown, recorded the greatest  $\Delta u$ . As observed for the westbound tunnel construction, although the lowest three piezometers in HP33 were interconnected, it seems that the immediate pore water pressure responses to eastbound tunnel construction were still measured independently.

### Response of HP34 piezometers (TBM2, period 4)

Pore water pressure changes measured within HP34 in response to eastbound tunnel construction, as shown in Figs 11(a)-11(c), were much smaller than those of HP32 and HP33, it being further away from TBM2 (18.6 m horizontally from its centre-line). Only the deepest sensor at  $z = -29$  m measured a gradual increase of pore water pressure up to +8 kPa during the passage of TBM2. Negligible changes were registered by the piezometers at other depths. The magnitude of the  $\Delta u$  response is even smaller than that measured within HP33 in response to the westbound tunnel construction (cf. Fig. 6). A likely reason for the smaller response at HP34 is the combined presence of the existing Central Line tunnel (see Fig. 1) and, perhaps more predominantly, the newly constructed Crossrail westbound tunnel. Both are stiffer than the ground and hence 'attract' more total stress changes induced by the eastbound tunnel construction. As a result the ground at HP34 would have experienced a smaller total stress change (and hence smaller excess pore water pressure) than the 'greenfield' ground at HP33 when the westbound tunnel was being constructed.

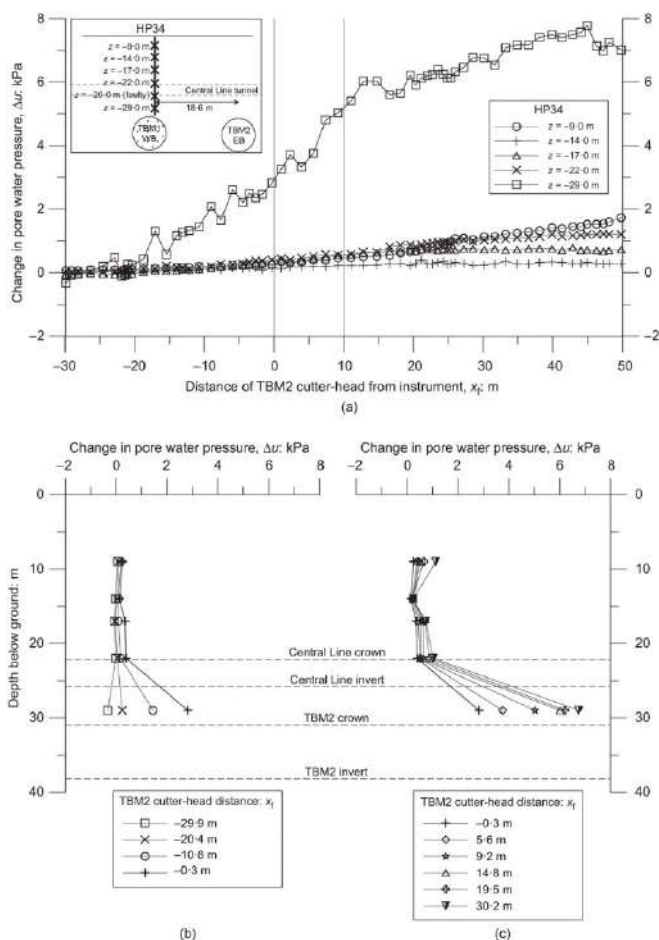


Fig. 11. Change in pore water pressure measured in piezometer HP34 in response to eastbound construction (period 4): (a) variation with TBM2 cutter-head distance; (b) depth profiles when the TBM2 cutter-head was approaching the instrument; (c) depth profile when TBM2 cutter-head was leaving the instrument

### Response of spade cells HP35, HP36, HP37 and HP39 (TBM2, period 4)

Data from the measurements of  $\Delta u$  and  $\Delta \sigma_h$  from the spade cells in response to the eastbound tunnel construction are presented in Fig. 12. The data-loggers serving HP36 and

HP37 became faulty during the tunnel construction period and so measurements were taken manually three to four times a day using a hand-held VW readout device and thus some critical readings might have been missed (compared with the hourly data logging). As shown in Fig. 12(a), values of  $\Delta u$  measured about 1.5 m either side of the eastbound tunnel extrados (HP35 and HP36) and about 2 m above the eastbound tunnel crown (HP39) showed almost the same pattern, with very slight increases (up to +5 kPa) as the cutter-head approached them (average face pressure = 200 kPa), followed by a consistent reduction of pore water pressure as TBM2 passed. The magnitudes of change were much larger than for TBM1, as with the TBM2 drive the relative distances were much closer, but the sense of change was completely opposite with decreasing pore water pressures observed compared with the increases seen when TBM1 passed. This suggests that the effects of unloading and shearing are much greater in the close vicinity of the TBM (TBM2 in this case, around which the instruments were closely clustered). Additionally, the rebound of pore water pressure, induced by the tail grouting as observed within the piezometers in HP32 and HP33 at corresponding  $y-z$  positions at  $x_f = 10$  m was not observed. In this case the pore water pressure responses measured at the spade cells do not seem as sensitive as those measured by the multi-level piezometers (HP32 to HP34). The reason for this is not known but might be associated with the contact condition (e.g. smeared or voided interface) between the soil and the piezometer filter on the spade surface. The final reduction in pore water pressure at these spade cell locations was about -100 kPa. Values of  $\Delta u$  measured by spade cell HP37 further away from TBM2 show responses of much smaller magnitude, being less than  $\pm 5$  kPa and so almost negligible. It is worth noting that, despite the difference in sensitivity, the magnitudes of the final change of pore water pressure after TBM2 has passed ( $x_f = 60$  m) measured by the deepest piezometer of HP33 and the spade cell HP39 (at the same relative position to TBM2) were comparable to each other, being about 100-115 kPa.

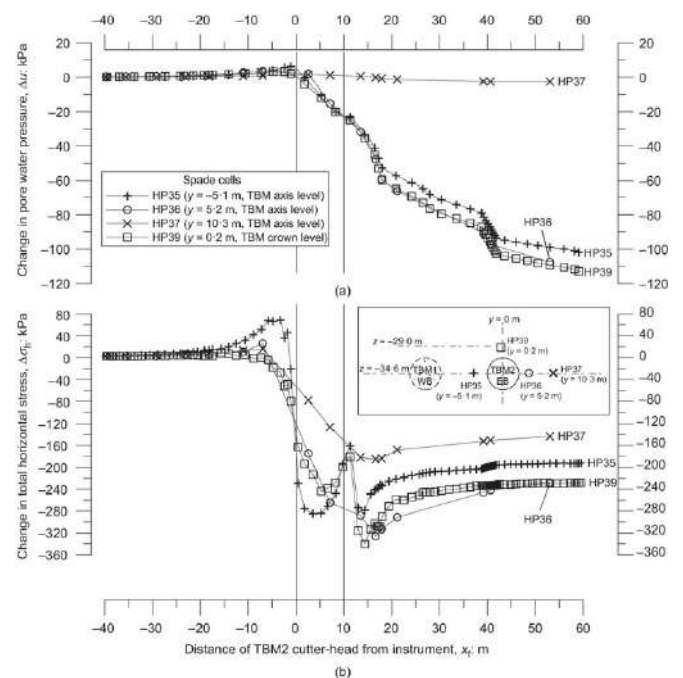


Fig. 12. Change in (a) pore water pressure and (b) total horizontal stress measured in spade cells HP35, HP36, HP37 and HP39 in response to eastbound construction (period 4)

There is a marked  $\Delta u$  reduction of up to 20 kPa measured in HP35, HP36 and HP39 at about  $x_f = 40$  m, which again is associated with a period when the TBM advance slowed down

(clustering of hourly readings). However, at the same time the corresponding  $\Delta\sigma_h$  values (transverse to the tunnel axis) measured by these spade cells were much less pronounced. This might imply that the marked changes in pore water pressure at  $x_f=40$  m originated mainly from the total horizontal stress change in the direction parallel to the tunnel axis.

An increase of total horizontal stress of up to +80 kPa was measured in HP35 prior to the cutter-head reaching the spade cells, probably as a result of the development of ground arching ahead of the approaching cutter-head (Fig. 12(b)). Very small total stress increases can be observed from the manual measurements at the other spade cell HP36, at the same offset but on the other (northern) side of the tunnel extrados, but no manual measurements were made at the time when the peak was observed in HP35. It therefore seems likely that greater  $\Delta\sigma_h$  values would have been observed at HP36, and perhaps HP37 (but judging from the trends, not to the same degree as HP35). However, no total horizontal stress increase was measured in the spade cell HP39 (hourly data-logged) directly above TBM2 crown, as might have been anticipated.

All four spade cells recorded a reduction in total horizontal stress as the TBM2 cutter-head reached them ( $x_f=0$  m), as a consequence of ground loss and stress relief due to the excavation. Readings from both HP35 and HP39 indicate a rebound of total stress between  $5\text{ m} < x_f < 10\text{ m}$  from tail grouting and the development of ground arching, reaching a peak, followed by a further drop between  $10\text{ m} < x_f < 15\text{ m}$  as the ground closed in towards the newly erected lining. It appears from the data available for HP36, and perhaps HP37, that the same trends would have been observed but have been missed because of the much lower frequency of manual measurements. Total stresses recovered partly as TBM2 advanced further from  $15\text{ m} < x_f < 20\text{ m}$  as a result of the tail grout setting and gaining stiffness, after which they stabilised.

### Further interpretation

Qualitative comparisons can again be made between trends in  $\Delta\sigma_h$  and the corresponding changes in displacement, referring to the observations of Wan et al. (2017b). Vertical displacements at axis level were small, being less than 6 mm, as measured from extensometer HP24 (Wan et al., 2017b: Fig. 8), which is at the same offset as HP36, and unlikely to have a significant influence on changes in horizontal total stress. It is interesting to note that the ground at the level of spade cell HP39, above the crown of TBM2, displaced downwards by about 23 mm, as measured by extensometer HP23. It seems likely that the spade cell displaced together with the ground resulting in negligible interaction effects from interface shearing. In terms of horizontal displacements, the reversal of ground movements at axis level that was observed for TBM1 is much less pronounced for comparative measurements for TBM2 (Wan et al., 2017b: Fig. 10(b) cf. Fig. 12(b)). Despite this, as described above, in terms of  $\Delta\sigma_h$  measurements, the rebound in total stress at axis level from tail grouting is very evident ( $5\text{ m} < x_f < 10\text{ m}$ , Fig. 12(b)). Horizontal displacements towards TBM2 as its tail passed inclinometer HP9 were greater than for TBM1 (measured within HP6 at same offset), being about 26 mm as opposed to 17 mm (refer to Figs 11 and 14 in the paper by Wan et al. (2017b)). This can be attributed to ground softening from the construction of TBM1, as discussed by the authors in the earlier paper. It is also evident from these same figures (Wan et al., 2017b: Figs. 11 and 14) how sensitive magnitudes of changes in displacement are to the distance from the tunnel extrados. Based on the observation above concerning rebound, a similar or even greater sensitivity would be expected in terms of stress changes.

The final reduction in total horizontal stress at spade cell HP36 ( $y=5.2$  m) was about -230 kPa; larger in magnitude than that at HP35 ( $y=-5.1$  m) which was about -190 kPa. This asymmetric response is most likely to be due to the construction and presence of the westbound tunnel, but could also be influenced by spade cell installation effects (e.g. deviation of spade orientation from the intended direction). Spade cell, HP37, also at axis level but further away from TBM2 ( $y=10.3$  m), recorded a smaller final reduction of about -140 kPa, while that at spade cell HP39, 2 m above the TBM2 crown, was about -230 kPa.

These measured net horizontal stress reductions of up to about -230 kPa, immediately above and at either side of the excavation, constitute up to one third of the estimated in situ total overburden stress at the tunnel axis level (650 kPa approximately) - that is, representing about 35% of it in the immediate short term.

### MECHANISMS OF EPBM TUNNELLING-INDUCED PORE WATER PRESSURE CHANGES AND GROUND ARCHING

By examining the immediate ground response in the close vicinity of the TBMs during their passage, a general pattern of pore water pressure changes can be formulated. The development of the pressure changes can be broadly divided into five stages/components in relation to the relative distance to the EPBM shield, as shown in Fig. 13 (typified by the response of the sensors at  $z=-31.0$  m and  $-37.2$  m in Fig. 9(a)). It is also instructive to relate these typical components to the effects of: (a) stress relief induced by ground losses at the cutter-head and tail void; (b) development of ground arching in front of the cutter-head (referred to as 'domed' arching) and along the shield body (referred to as 'longitudinal' arching) over softened ground that was subjected to greater ground losses; and (c) tail grout pressure compressing the ground around the tail skin. These effects and the postulated development of ground arching at different positions of an advancing EPBM are shown schematically in Fig. 14.

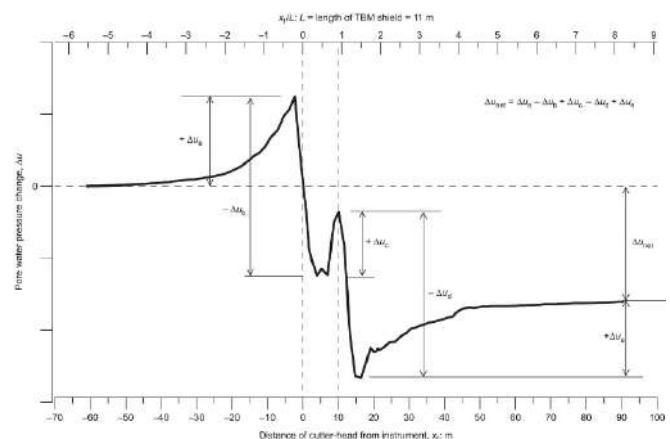


Fig. 13. Typical components of pore water pressure changes in relation to EPBM operations

The five components of pore water pressure changes, as shown in Fig. 13, the ranges over which they develop and their main causes, as postulated in Fig. 14, are described below.

- (a) The pore water pressure increases by an amount of  $+\Delta u_a$  when the cutter-head approaches, first due to the development of the 'domed' arching and then the 'longitudinal' arching around the cutter-head ( $x_f < -2$  m approximately).

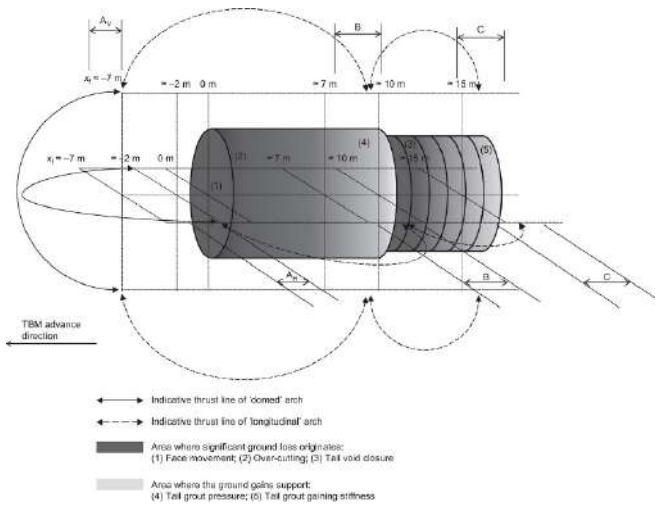


Fig. 14. Schematic representation of development of ground arching around TBM shield

- (b) It is followed by a reduction of  $-\Delta u_b$  induced by the stress relief as the cutter-head excavates and over-cuts the ground in the close proximity of the instrument location ( $-2\text{ m} < x_f < 5\text{ m}$  approximately).
- (c) The pore water pressure then undergoes a rebound of  $+\Delta u_c$  induced by the application of tail grout pressure and also development of the 'longitudinal' arch (occurring in advance of the tail skin,  $7\text{ m} < x_f < 10\text{ m}$  approximately).
- (d) As the shield tail progresses beyond the instrument, the pressure drops further by  $-\Delta u_d$  induced by the stress relief associated with the tail void closure ( $10\text{ m} < x_f < 15\text{ m}$  approximately).
- (e) Finally, the pressure recovers partly by  $+\Delta u_e$  upon the development of a second 'longitudinal' arching mechanism behind the shield tail on the tunnel linings after the tail grout sets and increases in stiffness ( $x_f > 15\text{ m}$ ).
- (f) The net pressure change  $\Delta u_{\text{net}}$  is the arithmetic sum of these components.

By further examining the pore water pressure changes in the vicinity of the eastbound tunnel construction measured by the piezometers in HP32 and HP33 (Fig. 15), the spatial variation in the transverse plane of these five components can be interpreted. The deepest two piezometers at  $z = -26.0\text{ m}$  and  $z = -29.1\text{ m}$  of HP33 were located vertically above the crown; the two piezometers at  $z = -31.0\text{ m}$  and  $z = -37.2\text{ m}$  of HP32 measure pore water pressures at the side of the tunnel; the deepest piezometer at  $z = -42.0\text{ m}$  of HP32 is assumed to measure pressures representative of that vertically below the tunnel invert.

The initial pore water pressure increase  $+\Delta u_a$  peaked at about  $x_f = -7\text{ m}$  above the crown and below the invert but at about  $x_f = -2\text{ m}$  at the side. The ranges over which the vertical and horizontal arching spring-lines would develop are marked as ranges  $A_v$  and  $A_h$ , respectively, in Figs 14 and 15, beyond which the ground would be greatly softened by the cutter-head face movement. Inspection of the field displacement measurements shows that there were greater measured vertical

displacements compared with the horizontal displacements at the same radial offset (see Fig 8(a) (HP23) and Fig. 10(a) in the paper by Wan et al. (2017b)), implying that the ground ahead of the cutter-head was softened to a larger

extent vertically than horizontally. It can therefore be inferred that the common arching spring-lines (the stiffer 'stationary' points in the ground) from which the 'domed' and 'longitudinal' arching mechanisms emanate in front of the cutter-head were further apart vertically than horizontally. This helps explain why, in front of the cutter-head, the measured pore water pressure above and below it started to drop earlier than at the side. Another potential explanation for this is that as the ground ahead of the cutter-head moved into the shield face, a proportion of the vertical stress above the projection of the tunnel crown was transferred to the sides, resulting in a reduction of the pore water pressure above the crown and an increase of the pore water pressure at the sides.

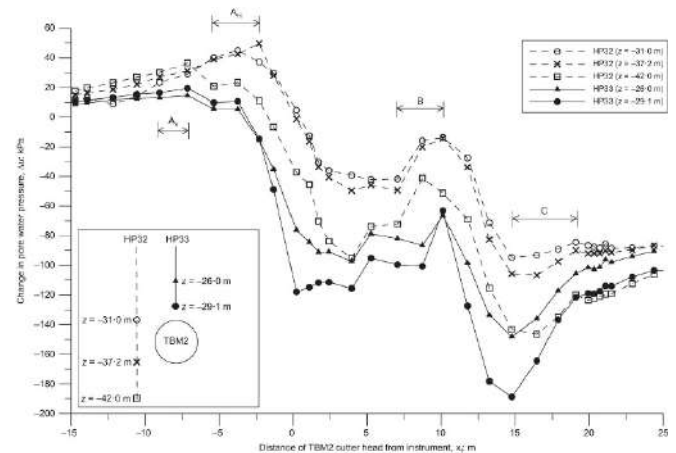


Fig. 15. Change in pore water pressure measured in piezometers HP32 and HP33 in the vicinity of the eastbound construction (period 4)

The subsequent pressure drop  $-\Delta u_b$  would continue until the instruments were roughly midway along the length of the shield body ( $x_f \approx 5\text{ m}$ ). The pressure rebound  $+\Delta u_c$  would then peak at between  $7\text{ m} < x_f < 10\text{ m}$  (referred to as range B in Figs 14 and 15) before the further pressure drop  $-\Delta u_d$  occurring until  $x_f \approx 15\text{ m}$  (range C). These ranges B and C correspond to the stiffer 'stationary' points in the ground from which the 'longitudinal' arching spring-lines behind the cutter-head were developed. It can be seen that behind the cutter-head ( $x_f > 0\text{ m}$ ), the same pattern of pore water pressure change seems to develop regardless of the measurement positions relative to the TBM in the transverse plane (above, below or at the side). This indicates that the tunnel axis, being at  $35\text{ m}$  or five times the excavation diameter below ground surface, was deep enough that the measured pore water pressure response showed no significant preference over any particular direction in the transverse plane. As such the pressure change (and ground movements) around the shield body (behind the cutter-head) and the erected linings would resemble that of a collapsing cylindrical cavity in an isotropic ground, as suggested by Mair & Taylor (1993).

Variations in the five different components of pore water pressure change with the radial distance from the tunnel axis, as well as the net pore water pressure change, are depicted in Figs 16(a)–16(f). In general, the magnitude of the pressure change decreases with increasing distance from the tunnel. The immediate response induced by the different stages of EPBM operation became insignificant at a radial distance greater than about three excavation diameters from the tunnel axis (i.e.  $6R$ ).

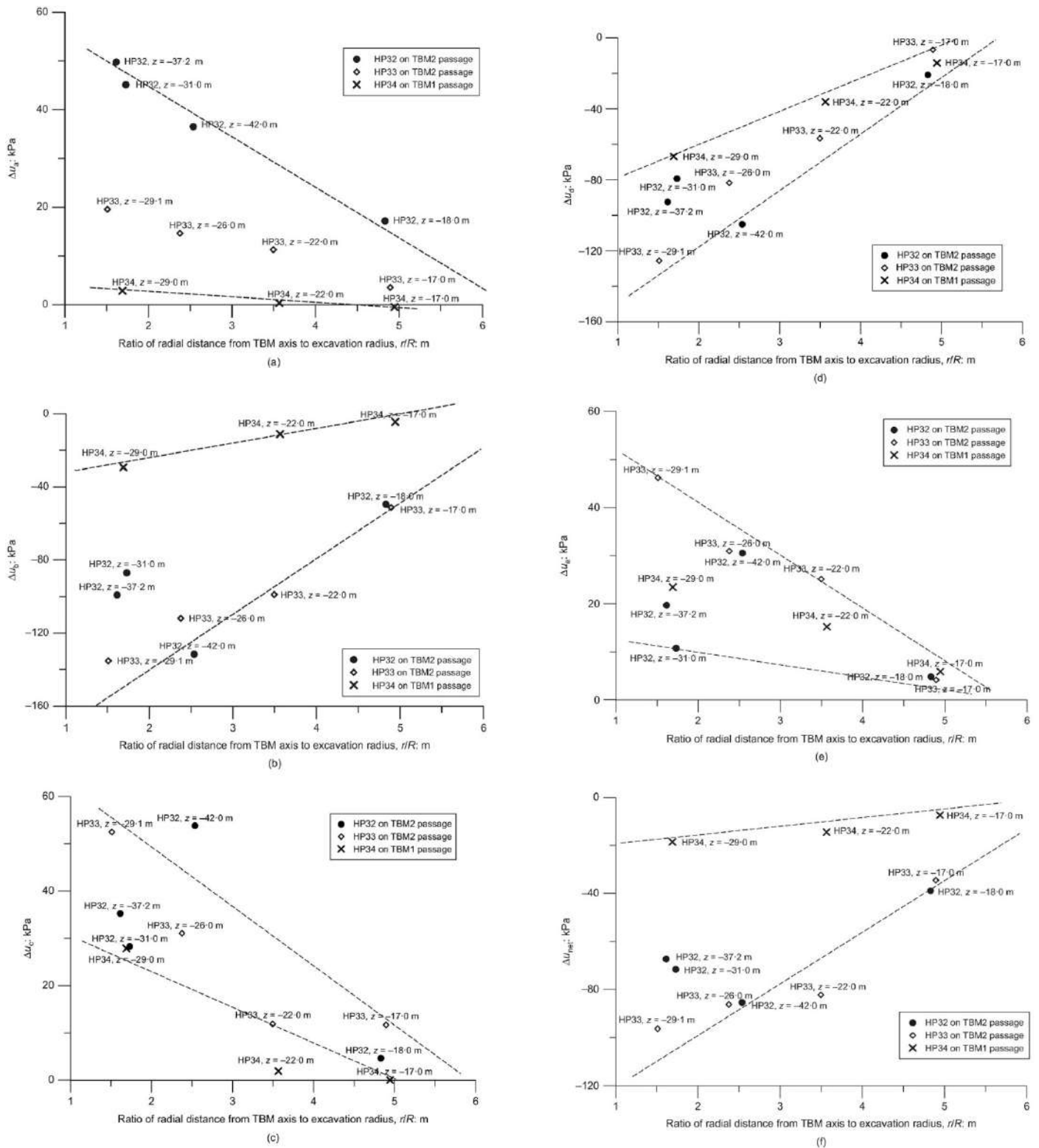


Fig. 16. Change of pore water pressure induced by: (a) TBM cutter-head approaching the instrument; (b) ground movement into TBM face and front of shield; (c) TBM tail approaching the instrument; (d) TBM tail void closure; (e) lining support. (f) Net change of pore water pressure induced by TBM passage

The lower bounds for the absolute responses of different components of pore water pressure changes are almost always formed by the data points for HP34 in Fig. 16. One reason for the smaller response at HP34 could be the presence of the existing Central Line tunnel 'attracting' more of the total stress change induced by the Crossrail tunnel construction. As a result the ground at HP34 would experience a

smaller total stress change (and hence excess pore water pressure) than the 'greenfield' ground at HP32 and HP33. In a similar manner, the presence of the existing Central Line tunnel also helped explain the smaller subsurface ground settlements measured at extensometer HP26 near the Central Line tunnel than those at the extensometer HP20 in the 'greenfield' ground during the westbound construction (Wan

et al., 2017b: Fig. 4) and also the smaller settlements measured at HP28 near the Central Line tunnel than at HP23 during the eastbound construction (Wan et al., 2017b: Fig. 8).

The non-isotropic response in front of the cutter-head in terms of the magnitudes of the component of pore water pressure increase ( $+\Delta u_a$ ) is evident from Fig. 16(a), with the piezometers at the side (HP32) measuring a consistently greater pressure increase than those above the crown (HP33) at the same radial distance from the tunnel. However, the magnitudes of the other components of pressure increase measured behind the cutter-head, as shown in Figs 16(b)–16(e), indicate a more isotropic response. This corroborates the suggestion that the ground response to the tunnelling operations behind the cutter-head resembles that of a collapsing (or expanding) cylindrical cavity in an isotropic medium.

The different components of pressure changes induced by both the westbound and eastbound construction measured by the VW piezometers HP32 (TBM2), HP33 (TBM2) and HP34 (TBM1) are summarised in Tables 3–5.

### SUMMARY AND CONCLUSIONS

The monitoring results of short-term pore water pressure and total horizontal stress changes induced by the twin-bore Crossrail tunnels measured at the Hyde Park instrumentation site have been presented and discussed. The key findings from the field measurement are as follows.

(a) The multi-level VW piezometers installed by the fully grouted method in boreholes near the tunnel construction were able to measure automatically, rapidly and independently the pore water pressure changes as the EPBM

passed the instruments (even in cases where instruments had a degree of interconnectivity).

(b) A clear pattern of developing pore water pressure and total horizontal stress changes was observed as the EPBMs approached and left the instruments, with a number of components associated with the relative position of the shield from the instrument clearly identified. Excess pore water pressure and total horizontal stress changes in response to the development of ground arching in front of and along the shield, cutter-head excavation, tail grouting, tail void closure and lining support were measured. These, together with the subsurface vertical and horizontal ground displacements measured by the rod extensometers and inclinometers near the tunnel construction described in the companion paper (Wan et al., 2017b), help with the understanding of the mechanisms of near-tunnel ground response to EPBM tunnel construction.

(c) In particular, the ground arching mechanism, first postulated by Terzaghi (1943) and subsequently investigated numerically and experimentally by other researchers, around an advancing EPBM in stiff London Clay has been clearly identified and validated for the first time by field monitoring of changes in pore water pressure.

(d) The measurements taken by the multi-level VW piezometers and the pushed-in spade cell piezometers show consistent trends of excess pore water pressure development. However, some aspects of response pertaining to the EPBM operations measured by the multilevel piezometers were not measured by the spade cells at the same relative positions to the tunnel construction, possibly due to the contact condition between the soil and the piezometer filter.

Table 3. Components of pore water pressure changes induced by eastbound construction (TBM2 passage) measured by HP32

Depth below ground: m	Radial distance from tunnel axis: m	Components of pore water pressure change: kPa					Net pore water pressure change $\Delta u_{net}$ : kPa
		$\Delta u_a$	$\Delta u_b$	$\Delta u_c$	$\Delta u_d$	$\Delta u_e$	
18.0	17.3	17.2	-49.5	4.7	-20.8	9.6	-38.9
31.0	6.2	45.1	-87.1	28.3	-79.3	21.5	-71.6
37.2	5.8	49.8	-99.2	35.2	-92.5	39.3	-67.3
42.0	9.1	36.5	-131.6	53.8	-105.1	61.0	-85.4

Table 4. Components of pore water pressure changes induced by eastbound construction (TBM2 passage) measured by HP33

Depth below ground: m	Radial distance from tunnel axis: m	Components of pore water pressure change: kPa					Net pore water pressure change $\Delta u_{net}$ : kPa
		$\Delta u_a$	$\Delta u_b$	$\Delta u_c$	$\Delta u_d$	$\Delta u_e$	
17.0	17.5	3.5	-51.3	11.7	-6.7	8.3	-34.5
22.0	12.5	11.3	-98.9	11.9	-56.6	50.2	-82.2
26.0	8.5	14.6	-112.0	31.1	-81.8	61.9	-86.2
29.1	5.4	19.6	-135.2	52.5	-125.7	92.5	-96.4

Table 5. Components of pore water pressure changes induced by westbound construction (TBM1 passage) measured by HP34

Depth below ground: m	Radial distance from tunnel axis: m	Components of pore water pressure change: kPa					Net pore water pressure change $\Delta u_{net}$ : kPa
		$\Delta u_a$	$\Delta u_b$	$\Delta u_c$	$\Delta u_d$	$\Delta u_e$	
17.0	17.7	-0.5	-4.5	0.0	-14.1	11.7	-7.4
22.0	12.7	0.4	-11.1	1.9	-36.0	30.4	-14.4
29.0	6.0	2.9	-29.3	27.9	-66.9	46.9	-18.6

- (e) The magnitudes of the different components of the pore water pressure changes associated with the EPBM operations were found to be decreasing with increasing distance from the excavation. The short-term effect of the EPBM construction in terms of the excess pore water pressure seems to be insignificant at a distance beyond three times the excavation diameter from the tunnel axis.
- (f) The presence of the existing Central Line tunnels near HP34 is likely to be the reason for the smaller magnitude of the short-term pore water pressure response to the westbound tunnel construction measured compared with those measured in 'greenfield' ground at HP32 and HP33 in response to the eastbound construction.

## ACKNOWLEDGEMENTS

The authors wish to acknowledge the Engineering and Physical Sciences Research Council (EPSRC) (EP/G063486/1) and Crossrail who were the major sponsors for this field component of the research project. Many thanks are due to the Imperial College research team, especially the Imperial College technician Mr Alan Bolsher, and those others who helped take the field measurements during the 24 h surveying periods. A thoughtful review of the instrumentation plan by Mr John Dunicliff is also greatly appreciated. The support provided by the Royal Parks, London Underground Limited and Westminster Council during the installation work is gratefully acknowledged. The specialist input and effort during the piezometer installation by itmsoil are very much appreciated. The authors are also grateful to the main joint venture contractors BFK, in particular Mr Ivor Thomas, for providing data and information relating to the EPBMs and their operation variables.

Discussion on this paper closes on 1 October 2019, for further details see p. ii.

## References

Afshan, S., Yu, J. B. Y., Standing, J. R., Vollum, R. L. & Potts, D.M. (2017). Ultimate capacity of a segmental grey cast iron tunnel lining ring subjected to large deformations. *Tunnelling Underground Space Technol.* 64, 74–84.

Avgerinos, V., Potts, D. M. & Standing, J. R. (2016). The use of kinematic hardening models to predict tunnelling-induced soil movements in London Clay. *Géotechnique* 66, No. 2, 106–120, <https://doi.org/10.1680/jgeot.15.P.035>.

Avgerinos, V., Potts, D. M. & Standing, J. R. (2017). Numerical investigation of the effects of tunnelling on existing tunnels. *Géotechnique* 67, No. 9, 808–822, <https://doi.org/10.1680/jgeot.SIP17.P.103>.

Avgerinos, V., Potts, D. M., Standing, J. R. & Wan, M. S.P. (2018). Predicting tunnelling-induced ground movements and interpreting field measurements using numerical analysis: Crossrail case study at Hyde Park. *Géotechnique* 68, No. 1, 31–49, <https://doi.org/10.1680/jgeot.16.P.219>.

Barratt, D. A. & Tyler, R. G. (1976). Measurements of ground movement and lining behaviour on the London Underground at Regents Park, Report no. LR684. Crowthorne, UK: Transport and Road Research Laboratory.

Burland, J. B., Simpson, B. & St John, H. D. (1979). Movements around excavations in London Clay. In *Proceedings of the 7<sup>th</sup> European conference on soil mechanics and foundation engineering*, vol. 1, pp. 13–29. London, UK: British Geotechnical Society.

Clayton, C. R. I., Hope, V. S., Heymann, G., Van der Berg, J. P. & Bica, A. V. D. (2000). Instrumentation for monitoring sprayed concrete lined soft ground tunnels. *Proceedings of the Institution of Civil Engineers – Geotechnical Engineering* 143, No. 3, 119–130, <https://doi.org/10.1680/genq.2000.143.3.119>.

Dival, S., Goodey, R. J. & Stallebrass, S. E. (2017). Twin-tunnelling induced changes to clay stiffness. *Géotechnique* 67, No. 10, 906–913, <https://doi.org/10.1680/jgeot.sip17.P.151>.

GCG (Geotechnical Consulting Group) (2009). *Geotechnical sectional interpretative report 1 & 2: Royal Oak to Liverpool Street*, Report no. 1D0101-G0G00-00549, Revision A, prepared for Cross London Rail Links Ltd. London, UK: Geotechnical Consulting Group LLP.

Glossop, N. H. (1978). *Soil deformations caused by soft-ground tunnelling*. Doctoral dissertation, Durham University, Durham, UK.

Grant, R. J. (1998). *Movements around a tunnel in two-layer ground*. Doctoral dissertation, City University London, London, UK.

Hwang, R. N., Wu, D. J. & Lee, C. J. (1995). Pore pressure response to shield tunnelling in soft clay. In *Proceedings of the South East Asian symposium on tunnelling and underground space development*, pp. 33–40. Tokyo, Japan: Japan Tunnelling Association.

Jiang, M. & Yin, Z. Y. (2012). Analysis of stress redistribution in soil and earth pressure on tunnel lining using the discrete element method. *Tunnelling Underground Space Technol.* 32, 251–259.

Jones, M. A. (2007). Rising groundwater in central London. *Water Sewerage J.* 4, 35–36.

King, C. (1981). *The stratigraphy of the London Basin and associated deposits*, Tertiary Research Special Paper. Rotterdam, the Netherlands: Backhuys.

Lee, C. J., Wu, B. R., Chen, H. T. & Chiang, K. H. (2006). Tunnel stability and arching effects during tunneling in soft clayey soil. *Tunnelling Underground Space Technol.* 21, No. 2, 119–132.

Lee, K. M., Ji, H. W., Shen, C. K., Liu, J. H. & Bai, T. H. (1999). Ground response to the construction of Shanghai metro tunnel-line 2. *Soils Found.* 39, No. 3, 113–134.

Lo, K. W., Chang, L. K., Leung, C. F., Lee, S. L., Makino, H. & Mihara, T. (1988). Field measurements at a multiple tunnel interaction site. *Proceedings of 2nd international symposium on field measurements in geomechanics*, Kobe, Japan, vol. 2, pp. 881–889. Rotterdam, the Netherlands: AA Balkema.

Macklin, S. R. & Field, G. R. (1999). The response of London Clay to full-face TBM tunnelling at West Ham, London. In *Urban ground engineering* (ed. B. Clarke), pp. 100–111. London, UK: Thomas Telford.

Mair, R. J. (1979). *Centrifugal modelling of tunnelling construction in soft clay*. PhD thesis, University of Cambridge, Cambridge, UK.

Mair, R. J. & Taylor, R. N. (1993). Predictions of clay behavior around tunnels using plasticity solutions. In *Predictive soil mechanics* (eds G. T. Houlsby and A. N. Schofield), pp. 449–463. London, UK: Thomas Telford.

- New, B. M. & Bowers, K. H. (1994). Ground movement model validation at the Heathrow Express trial tunnel. In *Tunnelling '94*, pp. 301–329. Dordrecht, the Netherlands: Springer.
- Nyren, R. (1998). Field measurements above twin tunnels in London Clay. PhD thesis, Imperial College, University of London, London, UK.
- Palmer, J. H. L. & Belshaw, D. J. (1980). Deformations and pore pressures in the vicinity of a precast, segmented, concrete-lined tunnel in clay. *Can. Geotech. J.* 17, No. 2, 174–184.
- Richards, D. J., Clark, J., Powrie, W. & Heymann, G. (2007). Performance of push-in pressure cells in overconsolidated clay. *Proceedings of the Institution of Civil Engineers – Geotechnical Engineering* 160, No. 1, 31–41, <https://doi.org/10.1680/geng.2007.160.1.31>.
- Ryley, M. D. & Carder, D. R. (1995). The performance of push-in spade cells installed in stiff clay. *Géotechnique* 45, No. 3, 533–539, <https://doi.org/10.1680/geot.1995.45.3.533>.
- Shirlaw, J. N. & Doran, S. R. (1988). Ground movements and settlements caused by tunnelling for the Singapore mass rapid transit system. In *Proceedings of Tunnelling '88*, pp. 295–314. London, UK: Institution of Mining and Metallurgy.
- Simpson, B., Blower, T., Craig, R. N. & Wilkinson, B. R. (1989). The engineering implications of rising groundwater in the deep aquifer beneath London, Special Publication 69. London, UK: Ciria.
- Standing, J. R. & Selemetas, D. (2013). Greenfield ground response to EPBM tunnelling in London Clay. *Géotechnique* 63, No. 12, 989–1007, <https://doi.org/10.1680/geot.12.P.154>.
- Standing, J. R., Potts, D. M., Vollum, R., Burland, J. B., Tsiamposi, A., Afshan, S., Yu, J. B. Y., Wan, M. S. P. & Avgerinos, V. (2015). Investigating the effect of tunnelling on existing tunnels. In *Proceedings of the conference on underground design and construction*, pp. 301–312. Hong Kong, PR China: Institute of Materials, Minerals and Mining (Hong Kong Branch).
- Tedd, P. & Charles, J. A. (1981). In situ measurement of horizontal stress in overconsolidated clay using push-in spade-shaped pressure cells. *Géotechnique* 31, No. 4, 554–558, <https://doi.org/10.1680/geot.1981.31.4.554>.
- Tedd, P. & Charles, J. A. (1983). Evaluation of push-in pressure cell results in stiff clay. In *Proceedings of the international symposium of soil and rock investigation by in-situ testing*, vol. 2, pp. 579–584. Paris, France: International Association for Engineering Geology.
- Tedd, P., Powell, J. J., Charles, J. A. & Uglow, I. M. (1989). In-situ measurements of earth pressures using push-in spade-shaped pressure cells – 10 years' experience. In *Geotechnical instrumentation in practice: purpose, performance and interpretation*, pp. 701–715. London, UK: Thomas Telford.
- Terzaghi, K. (1943). *Theoretical soil mechanics*. New York, NY, USA: John Wiley and Sons.
- Tsiampousi, A., Yu, J., Standing, J. R., Vollum, R. & Potts, D. M. (2017). Behaviour of bolted cast iron joints. *Tunnelling Underground Space Technol.* 68, 113–129.
- Wan, M. S. P. (2014). Field monitoring of ground response to EPBM tunnelling close to existing tunnels in London Clay. PhD thesis, Imperial College London, London, UK.
- Wan, M. S. P. & Standing, J. R. (2014a). Lessons learnt from installation of field instrumentation. *Proceedings of the Institution of Civil Engineers – Geotechnical Engineering* 167, No. 5, 491–506, <https://doi.org/10.1680/geng.13.00054>.
- Wan, M. S. P. & Standing, J. R. (2014b). Field measurement by fully grouted vibrating wire piezometers. *Proceedings of the Institution of Civil Engineers – Geotechnical Engineering* 167, No. 6, 547–564, <https://doi.org/10.1680/geng.13.00153>.
- Wan, M. S. P., Standing, J. R., Potts, D.M. & Burland, J. B. (2017a). Measured short-term ground surface response to EPBM tunnelling in London Clay. *Géotechnique* 67, No. 5, 420–445, <https://doi.org/10.1680/jgeot.16.P.099>.
- Wan, M. S. P., Standing, J. R., Potts, D.M. & Burland, J. B. (2017b). Measured short-term subsurface ground response to EPBM tunnelling in London Clay. *Géotechnique* 67, No. 9, 748–779, <https://doi.org/10.1680/jgeot.SIP17.P.148>.
- Wright, P. J. (2013). Validation of soil parameters for deep tube tunnel assessment. *Proceedings of the Institution of Civil Engineers – Geotechnical Engineering* 166, No. 1, 18–30, <https://doi.org/10.1680/geng.9.00095>.
- Yi, X., Rowe, R. K. & Lee, K. M. (1993). Observed and calculated pore pressures and deformations induced by an earth balance shield. *Can. Geotech. J.* 30, No. 3, 476–490.
- Yu, J., Standing, J. R., Vollum, R., Potts, D. M. & Burland, J. B. (2017). Experimental investigations of bolted segmental grey cast iron lining behaviour. *Tunnelling Underground Space Technol.* 61, 161–178.

**Published Online:** April 12, 2019

<https://www.icervirtualibrary.com/doi/10.1680/jgeot.17.P.309>

## Rehabilitation of Brougham Castle Bridge, UK

**David Wiggins** BSc(Hons), PhD, IEng, MICE, Senior Conservation-Accredited Engineer, Curtins, Kendal, UK

**Kiera Mudd** MEng(Hons), Engineer, Curtins, Leeds, UK

**Matthew Healey** HNC, ONC, Contracts Director, Civil Engineering, Metcalfe Plant Hire Ltd, Penrith, UK

Brougham Castle Bridge is a three-span masonry arch highway bridge that has suffered significant scour damage to foundations and substructure with referred damage through the superstructure. This paper presents an engineer's account of the appraisal, investigation, assessment of structural action and the design and execution of repairs for stabilising the structure. The analytical tool employed to interpret the flow of force was a thrust-line graphical equilibrium analysis. It will be demonstrated that this analytical approach accords with the observed structural pathology, thus giving a clear understanding as to where the loads are going, that they may be effectively grappled with. Through thrust-line analysis, continued stability could be demonstrated despite substantial changes in the foundation conditions. It seems fitting that this efficient, robust and confidence-building tool is the same used by the engineers who originally designed many of these bridges. Using this 'historical approach', a successful intervention was executed; initially emergency stabilisation work to save the bridge from collapse and latterly permanent rehabilitation works to bring the bridge back into service in advance of the upcoming winter floods.

### Notation

$H$	horizontal force component
$H$	height
$L$	length
$M$	moment
$n$	integer
$R_v$	resultant vertical force
$V$	vertical force component
$W$	weight
$x$	horizontal distance
$y$	vertical distance

### 1. Introduction

Brougham Castle Bridge was constructed between 1811 and 1813 as part of the turnpike road system strengthening links between Penrith and Appleby (Historic England, 2018a). It is a three-span masonry arch bridge, of a total crossing length of 43 m, over the River Eamont on an 'S-bend' just downstream of the confluence between the River Eamont and the River Lowther. The build form is typical of that period (Rudock, 2009), comprising mass stone block spread foundations, ashlar facing masonry to the piers and cutwaters containing a rough rubble core. Segmental voussoir arches spring from carved skewbacks atop ashlar capping slabs over the pier heads, with rubble and soil fill over, between traditional masonry spandrels and parapets. The stone is Red Permian Penrith Sandstone of typical characteristics: density 2340 kg/m<sup>3</sup>, compressive strength c. 100 N/mm<sup>2</sup> and porosity c. 10–15% (Cumbrian Stone, 2016).

The bridge is Grade II listed and interfaces with a Scheduled Ancient Monument, Brougham Castle, at its southern abutment, which is the site of the historic Roman fort Brocavum, from which Brougham takes its name (Historic England, 2018b). In the winter of 2015, Storm Desmond struck Cumbria, leading to widespread damage across the county's rich masonry heritage (McIntyre, 2018). The Cumbria Infrastructure Recovery Programme (CIRP) was established to tackle

the problem, as presented by Mathews and Hardman (2017).

The damage mechanism at Brougham Castle Bridge is as follows

- constriction scour under extreme flow volume combining with local scour at the northern pier, which led to the undermining of the upstream cutwater
- subsequent collapse of the cutwater
- progressive collapse of approximately the upstream third of the pier and incoming arch barrels.

Figure 1 presents a view of the damaged bridge.



Figure 1. View of the damaged bridge from the northern bank looking south

The rehabilitation project was commissioned through the CIRP on a design-and-build New Engineering Contract 3 basis, awarded to Metcalfe Plant Hire Ltd (Civil Engineering Division), who engaged Curtins as structural engineers. The project was undertaken in two stages – an initial temporary stabilization followed by permanent rehabilitation works the following year.

The bridge was in a dangerous condition and presented significant safety challenges. It was closed to all public and traffic. Risks were assessed and managed on the basis of phased incremental working proximity, as unknowns were gradually removed and load paths were restored. Diagnosis of current and remaining load paths was central to managing risk. Real-time movement monitoring comprising vibration and tilt sensors attached to key elements of the bridge formed part of this approach. This ensured that construction activity did not worsen the structural condition and would give warning of further movement, were it to occur. Threshold values were determined as follows (BSI, 2007, 2009; Ciria, 1992)

- ruinous elements – 2 mm/s peak particle velocity (PPV)
- wider bridge – 10 mm/s PPV
- 1° of tilt for bodies of overhanging masonry.

### 2. Appraisal of the damaged bridge

A detailed visual structural condition appraisal was the first stage in assessment and yielded the following primary observations

- (a) northern and southern abutments largely unaffected
- (b) southern pier apparently unaffected
- (c) southern arch span apparently unaffected

- (d) central span segmental arch elevational geometry largely unaffected
- (e) central span partial collapse of barrel on plan
- (f) northern arch span partial collapse of barrel on plan
- (g) northern cutwater collapsed, washed away
- (h) northern pier laterally undercut down the northern flank and transversely undercut at the upstream end
- (i) apparent tilt of northern pier downwards in the upstream direction
- (j) prominent crack along the bed joint at the springer of the northern arch as it bears onto the skewback on the pier
- (k) prominent vertical crack up the remaining length of northern pier some 1.5 m back from the upstream face on the southern flank
- (l) parapet flat-arching over the collapsed pier, crown to crown, spalling of arrises and evidence of longitudinal buckling observed under suspected high thrust.

Figure 2 presents a striking visual record of the bridge in the damaged state.

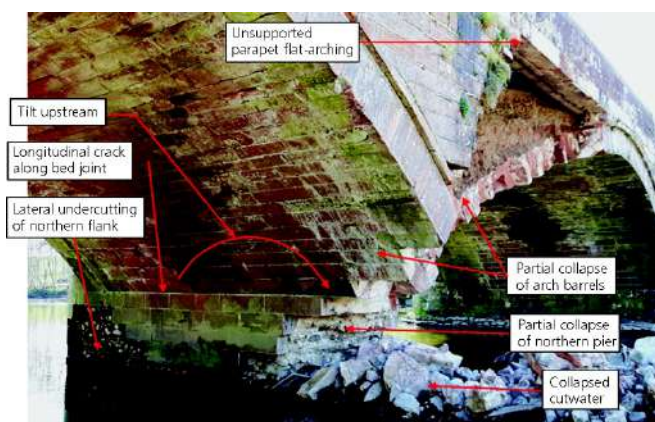


Figure 2. Brougham Bridge partial collapse of northern pier, viewed looking south

The bridge had seemingly halted in deterioration since the floodwaters subsided and in essence stood still for around 4 months until the time of assessment. It had self-evidently found a state of equilibrium with the change in support conditions. The objective of the structural condition appraisal was to determine the answers to the following questions.

- Why was it still standing up?
- Where were the load paths going?
- What were the magnitudes of those loads?
- What was the remaining margin of safety under dead-load conditions?

Answers to these questions would inform the design of the temporary stabilisation work and execution strategy. A measured survey was initially made using photogrammetry. This recorded the physical geometry of the damaged bridge from which the stability assessment was then made. This informed the magnitude of the upstream lean of the pier, approximately 150 mm (cf. observation (i)). It was also revealed that the geometries of the incoming arch barrels did not fit round imperial numbers, suggesting some deformation, possibly historic and/or recent in activity. By comparison, the southern span fitted imperial units, implying that a proportion of the discord between metric and imperial geometries of the north and central spans was related to the damage to the pier.

An equilibrium assessment using traditional graphic statics (thrust lines and force vectors) was used to interpret the structural behaviour. Clearly, the damage occurs in three dimensions, so the problem was broken down and considered two-dimensional (2D) both on elevation/vertical section and on plan. The various outcomes were then reconciled to build a three-dimensional (3D) understanding of the bridge's structural behaviour.

### 2.1 Introduction to thrust-line equilibrium analysis

Thrust-line analysis is based on three fundamental principles (Heyman, 1969).

- Masonry has unlimited compressive strength.
- Sliding between the masonry units does not occur.
- Masonry has zero tensile strength.

It is typical for masonry arches under dead loads to crack slightly at the crown (hinge opening towards the intrados) and at the springings (hinge opening towards the extrados), hence forming a three-pin statically determinate structure (Figure 3). The line of thrust passes through these hinges. The hinge locations can adjust to accommodate imposed load or to find support if damage is sustained. In order to calculate the line of thrust and its magnitude, funicular polygons can be drawn and the line of thrust plotted graphically. If the arch can be shown to have a valid load path which is contained entirely within the masonry, the structure is considered to be safe. The technique is described in detail by Heyman (1969, 1982, 1996).

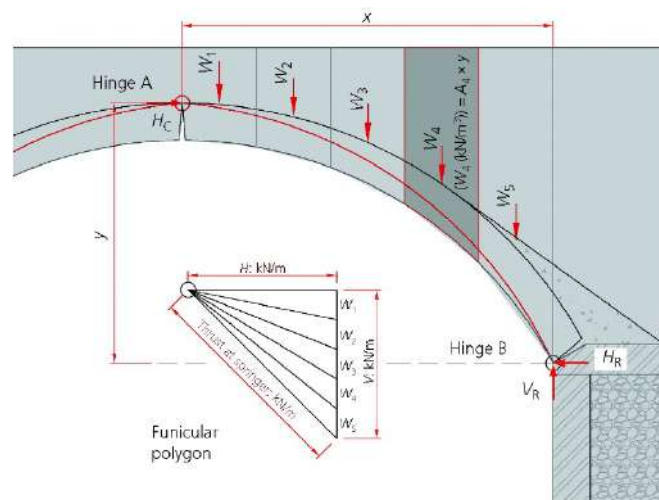


Figure 3. Thrust-line analysis of half-arch in minimum-thrust dead-load conditions

One particular strength of this technique is that it does not require detailed knowledge of foundation conditions (Harvey, 2012a) which, particularly in this context, was unknowable at this stage.

The method recognises the structural behaviour of historic masonry as an assemblage of dry-jointed masonry units, drawing strength and stability from its mass and geometrical form. In essence, this means that an arch barrel is fundamentally a thick, laterally loaded masonry wall curved about its axis. This qualitative understanding was central to structural diagnosis of the flow of force in the damaged state (Harvey, 2013).

Design information was determined as follows

- stone masonry density 23.5 kN/m<sup>3</sup>

- fill density approximately 17 kN/m<sup>3</sup>
- average estimate of masonry and fill combined density c. 21 kN/m<sup>3</sup>
- dead-load-only assessment conditions.

## 2.2 Longitudinal stability

To begin, the natural 'minimum-thrust' behaviour of the bridge was assessed in the undamaged original state, presented in Figure 4. The force components of thrusts on the northern pier were determined to be

$$1. \sum M_{\text{crown}} = 0$$

where  $H_C = H_R$  for equilibrium and  $\sum V$  is known

$$0 = \sum [(W_1 \times x_1) + (W_2 \times x_2) + (W_n \times x_n)]$$

$$2. + (H_R \times y) - (V_R \times x)$$

left-hand (northern) arch:  $H = 200$  kN/m;  $V = 240$  kN/m

right-hand (central) arch:  $H = 240$  kN/m;  $V = 300$  kN/m

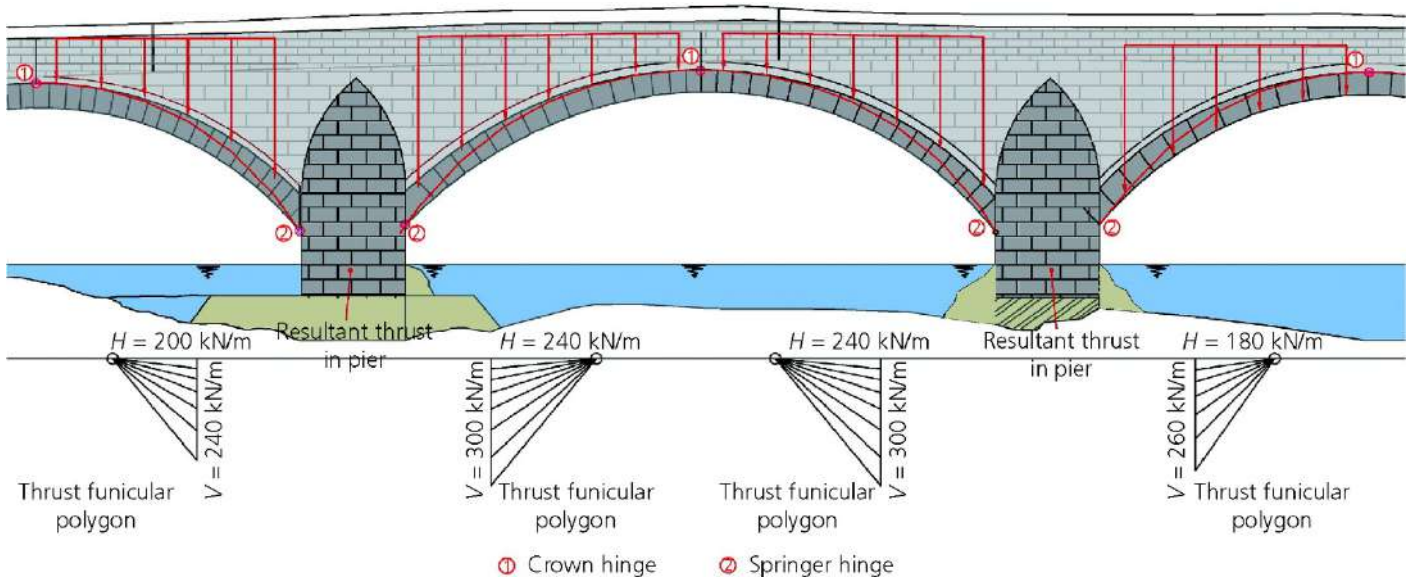
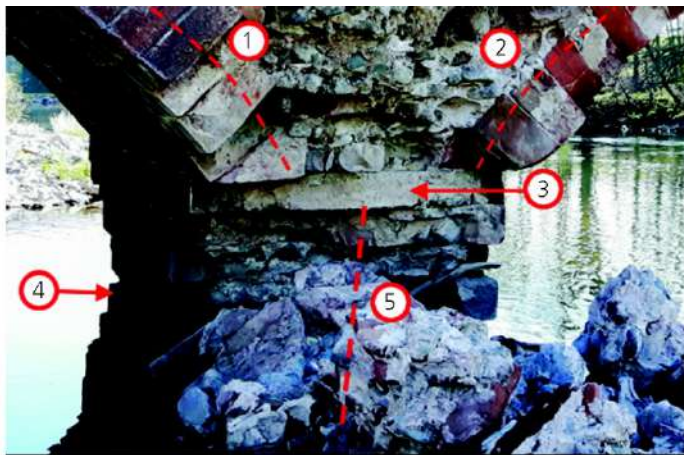
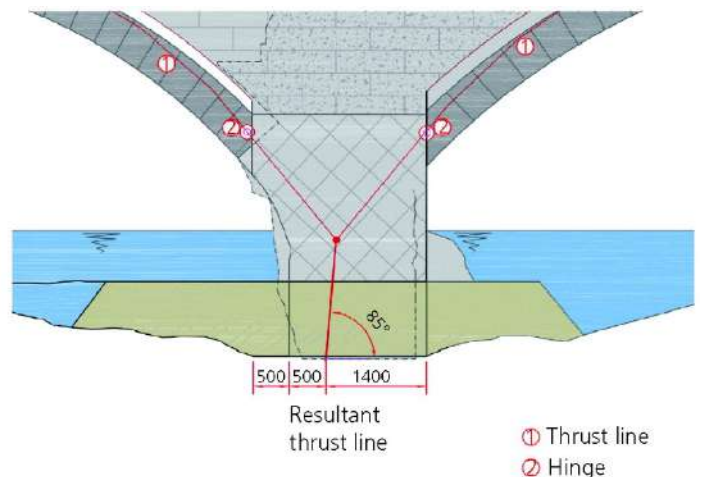


Figure 4. Longitudinal thrust-line analysis of thrust magnitudes in bridge



- ① LH arch thrust
- ② RH arch thrust
- ③ Pier capping slab
- ④ Lateral undercutting to LH flank
- ⑤ Resolved thrust in pier

(a)



(b)

Figure 5. Thrust and counterthrust force resolution at the pier head. Note the springer hinge lifts from the minimum-thrust position to find stiff support further over the pier head. LH, left hand; RH, right hand. (a) photograph of 'physical cross-section' through pier with structural action superimposed, (b) thrust-line equilibrium assessment of Figure 5(a)

Introducing the observed defect of the lateral undercutting to the northern flank of the pier and in recognition of the crack at this position (opening of the bed joint along the springer block), the springer hinge was lifted and lengthened to reach

further over the pier for the arch to find the support (Figure 5).

Note the presence of the stocky ashlar capping slab beneath the skewbacks (Figure 5(a)). This was judged to provide a stiff load path to accept the thrust from the arch barrel and spread it across the rubble fill core (Harvey, 2012b, 2013). This is an exception to the norm whereby the tightly jointed ashlar facing masonry carries the structural load, following the stiffest path – c. an order of magnitude stiffer than the lime-concrete rubble core (see the paper or Cassinello (2006)). The resolved thrust/counterthrust relationship between the incoming arches was assessed in a 2D section, as presented in Figure 5(b).

In vertical section/elevation, the pier and incoming arches were determined to be stable in the longitudinal direction by satisfactory resolution of thrusts.

### 2.3 Plan stability

Next, the observed defect of partial collapse of the northern pier was introduced. The behaviour of the incoming arches on plan was considered as follows.

- The nearside half of the central arch span was imagined as a masonry corbel (curved about its axis), loaded on

top with a preload representing the horizontal thrust force component at the crown.

- The presence of the crack (cf. observation (j)) was introduced, and the idealised corbel dimensions are presented in Figure 6(a). The root cause of the crack (j) was not conclusively proved although it was suspected as being local differential settlement over the scour hole on the upstream end; the ashlar pier flank shearing under high load until foundation support was reprovided.
- Tracking the thrust down through the corbel demonstrated a satisfactory possible load path.
- The remaining extent of the arch barrel on the downstream side of the crack was considered to arch 'normally' (approximated as metre-strip lengths between piers).
- An alternative possibility was considered whereby the thrust could skew on plan between the piers, presented in Figure 6(b).
- The actual position of the thrust is essentially unknowable (Heyman, 1996), but two possible load paths were demonstrated: each could be refined in detail, with a range of stable possibilities in between, so the plan stability was judged to be satisfactory.
- The left-hand (northern) arch on the plan was considered to adopt a similar structural behaviour, and the damage on the plan was accounted for in the overall assessment.

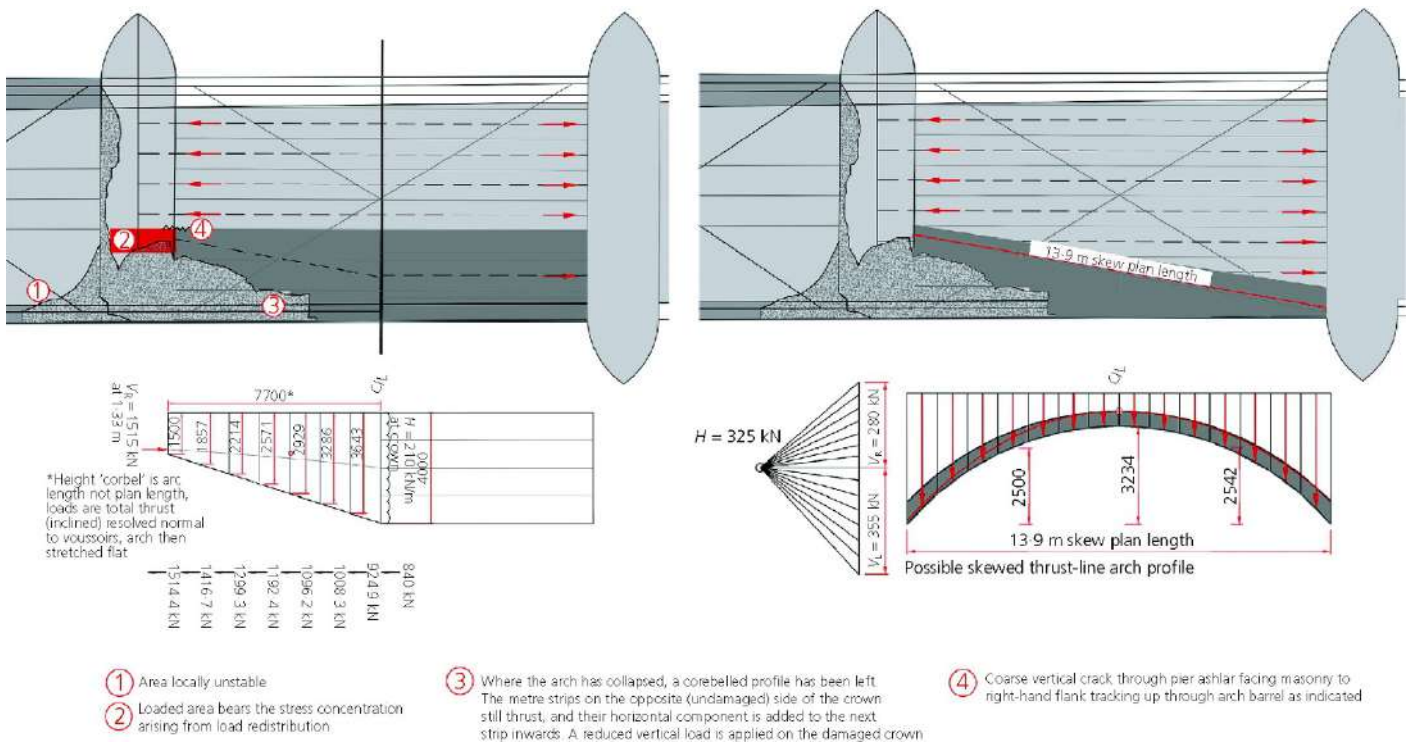


Figure 6. (a, b) Idealisations of the barrel partial collapse and the flow of force in the damaged state. Northern span considered to arch on plan in a similar manner to find support from the damaged pier

### 2.4 Transverse stability

The stability of the pier was then checked in the transverse direction, bringing in the load concentration from the plan-arching behaviour of the incoming arches and combining this with the undercutting to its upstream end. Again, the behaviour of a masonry corbel was used to interpret the load paths and stability. Figure 7 presents the idealised load diagram.

$$\sum M_{\text{heel}} = 0$$

$$0 = [(275 \text{ t} \times 2.5 \text{ m}) + (100 \text{ t} \times 4 \text{ m}) + (100 \text{ t} \times 5.5 \text{ m}) + (80 \text{ t} \times 3 \text{ m})] - (x \times V_R)$$

where  $V_R = 550 \text{ t}$  and  $x = 3.4 \text{ m}$  from the heel (on the edge of the middle third).



The parapet arching overhead was then lifted off block by block by means of a hydraulic grab, the masonry units palletised and reclaimed where sound for later reinstatement. The bridge was reassessed, and the movement monitoring confirmed that it remained at rest: the installation of the temporary cutwater and pier shoring works could begin.

Precast concrete 'Lego blocks' were lifted in from distance to form a shutter. Concrete was pumped in from safety, which then engaged the overhanging upstream face of the pier. Once early strength was reached, close-quarters access could be achieved to pack tightly the unsupported ashlar load-bearing facing masonry against the new concrete. Large-section granite rock armour was then used to form a 'falling protection' apron around the pier, and the bridge was left for the winter (Figure 8). Monitoring continued through the use of data loggers until the summer environment agency (EA) working window for the permanent reinstatement works, proving that the temporary stabilisation had arrested any further movement.

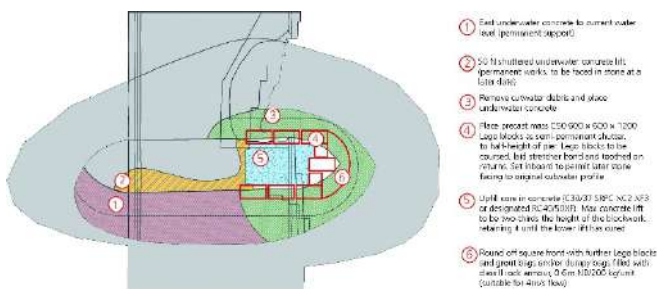


Figure 8 Plan survey on north pier temporary stabilisation works as completed prior to winter 2016. ND, nominal dimension; SRPC, sulfate-resisting Portland cement

## 5. Permanent rehabilitation works

The 'breathing space' break in the contract allowed a detailed study of the bridge's history. This revealed that a similar partial collapse issue had occurred, washing away one of the upstream cutwaters entirely in 1899 (Curwen, 1932). Which cutwater collapsed at that time is not certain, although it seems likely that it would be the same one: repair access would have been limited, making it difficult to achieve a robust repair at that time. Ultimately, it is believed that this led to the residual weakness inherent in the pier, which was then exploited by the Storm Desmond flood event some 120 years on.

The permanent reinstatement works required listed building consent and scheduled ancient monument consent in addition to extension of the EA working permit. From a conservation engineering perspective, there was clearly an imperative to save the bridge as a designated historic asset, but the nature of the repair gave particular focus to the following aspects

- to reinstate the original structural action (an arching gravity-masonry structure) – that is, working with the structure as opposed to against it
- to make faithful use of traditional building skills and materials which would be technically compatible with the existing and replacement masonry fabric
- to reinstate the character and appearance of the bridge, complementing the overall setting (its interrelationship with Brougham Castle to the south bank).

A site investigation was undertaken by way of microcoring down through the piers to confirm the relative positions of the foundation, formation material and bedrock. It demonstrated that the mass stone spread footing was founded on a layer of granular riverbed overlying weathered sandstone

bedrock (Figure 9). The root of the problem was hence demonstrated – a scour-susceptible formation.

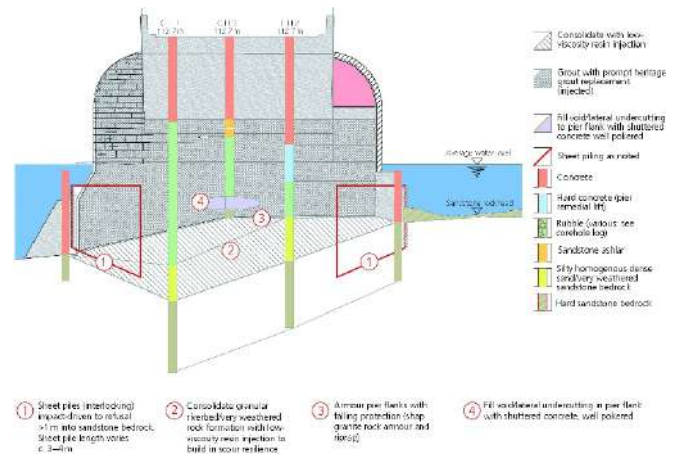


Figure 9 Transverse section through pier showing formation strata and foundation repair work requirements

Remedial design sought to

- fill the remaining voids in the formation and bridge sub-structure
- provide a physical barrier against local scour at both upstream and downstream cutwaters
- consolidate loose scour-susceptible formation material (to tackle constriction scour)
- provide a scour-resilient falling-protection apron for resilience to pier flanks.

The remedial detail adopted employed interlocking sheet piles driven to refusal in weathered bedrock, grouting with low-viscosity resin to bind the riverbed material and a rock armour apron. Design principles were informed by the publications by the Construction Industry Research and Information Association (Ciria, 2015, 2006) and Page (1996).

The structural repair of the pier employed techniques presented by Sowden (1990), broadly comprising anchoring of the pier stabilisation concrete into the remaining body of masonry, stitching of the ashlar facing masonry through the pier, grouting of the voided rubble core and reinstating the ashlar stone masonry where lost, including the construction of a new cutwater. The grouting served to help regulate the difference in stiffness between the rough rubble core and the concrete pier fill, avoiding longer-term crack propagation at the interface.

Repair of the partially collapsed arch barrel to the central span required a centring system (Figure 10). This required temporary spread foundations, which were bedded in by the jacks using the weight of the bridge as kentledge. The centring system was used as not only a passive formwork, but also an 'active' support, hydraulically jacking the barrel once the fill was removed to unlock the thrust binding the voussoirs together. This eased the tooth-bonding of the replacement voussoirs into the remaining barrel. The preload in the jacks then was then removed to lock the replacement units into place (Figure 11).

Real-time movement monitoring was employed throughout the jacking activities. The piers were laterally braced by the centring system using waling beams off the bottom chord, to permit safe removal of the fill over the central span, keeping the thrusts safely resolved within the piers during the jacking activities.



Figure 10 Centring system by temporary works specialist Mabey Contracting being rolled into position on girders on temporary spread foundations formed in the riverbed, viewed from downstream end. Note the hydraulic jacks between the tie-beam and concrete foundation bypassing the girders. The centring truss nodes each have a screw jack to fine-tune the shape up to engage the barrel intrados. Timber folding wedges are then driven into place to engage the masonry fully

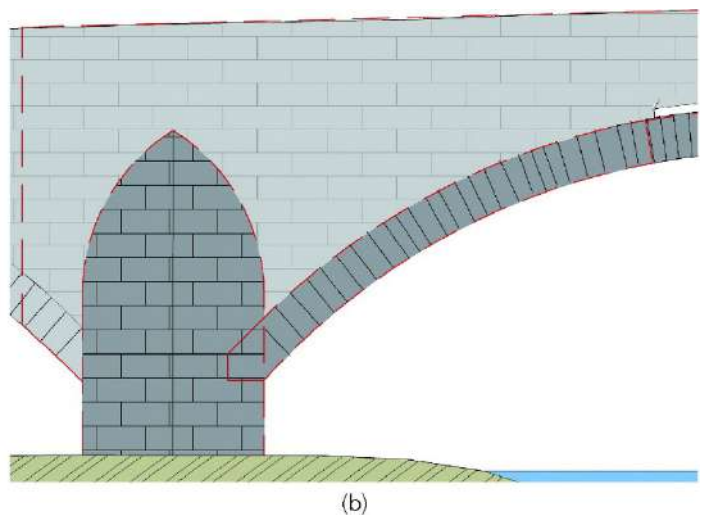
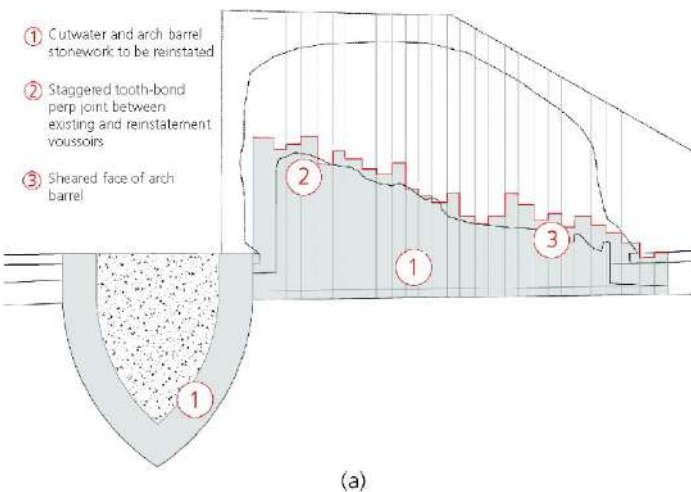


Figure 11 Arch barrel repair details: (a) plan and (b) sectional views

- Vicat Prompt for context (a) – [natural cement]
- Prompt/natural hydraulic lime (NHL) blended hydraulic binder for context (b) – [C3 hydraulic lime].

The low lime content of the Prompt/NHL hybrid binder was recompensated for through the aggregate, by blending crushed CL90 limestone into the mix. This achieved a strong, quick-setting, durable mortar in wet conditions, yet with a high uncombined lime content which allows the mortar to dry out and preserve the masonry units (Wiggins, 2018a).

For microcontent (c), a more sacrificial mortar was designed comprising the following mix constituents

- CL90 quicklime/NHL blended hydraulic binder for context (c) – [C2 hydraulic lime].

The mortars were designed to replicate the indigenous hydraulic limes used in bridge-building mortars as recorded in Cowper's UK hydraulic lime classification (Cowper, 1927).

## 7. Rehabilitation

The repair design was demonstrated to support the original

Spandrel and parapet walls were rebuilt in stone to match the southern span details. A Lytag saddle was placed over the central span to strengthen the arch. Lytag was employed as it had a closer modulus to masonry than dense concrete (Wilmers, 2012). A sawn construction joint was introduced to the concrete saddle at the crown to encourage the formation of the natural hinge at the crown, rather than cracking unpredictably.

## 6. Fabric repair and conservation

Fabric repair was designed with compatible lime mortars (Henry and Stewart, 2012; Pavia, 2006; Wiggins, 2018a, 2018b) in recognition of the various microcontexts at hand, namely

- pointing mortar
- cyclic wet and dry pier/cutwater mortar
- humid superstructure mortar.

For (a) and (b), a hydraulic lime mortar was designed for rapid-set capability in wet conditions while maintaining technical compatibility with the stone masonry, comprising the following constituents

17.5 t restricted access using the Archie-M thrust-line bridge assessment program. The program uses graphic statics to interpret masonry bridge behaviour under dead and live loads including rolling point loads (e.g. lorry axle in the Highways Agency (2001) standard). Figure 12 presents a graphic of the thrust-line feedback under a rolling point load at an onerous quarter-point position.

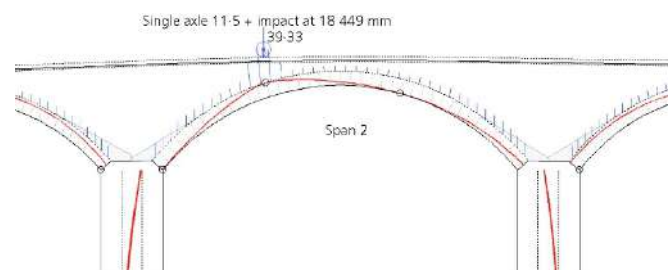


Figure 12 Central span under quarter-point loading with passive response from unloaded arches

The final stage in rehabilitation was to undertake a load test to the procedure outlined in the Highways Agency (1994) standard, broadly comprising a loaded aggregate lorry set to

position its rear axle over defined points on the bridge (e.g. pier head, arch quarter-point, crown.) while a digital theodolite monitored preset targets positioned on the arch barrel over time. The test is a bit of a 'blunt instrument' (it measures the face voussoirs of the barrel only); however, it was instructive insofar as appraising deformation under a given load for the repaired area. The repaired pier recorded zero deformation under load. The arch barrel initially recorded some 8 mm settlement of the first voussoir bearing on the embedded skewback and around 5 mm at the quarter-point of the rebuilt barrel section.

The deformation stopped after the first 5 min loading period and remained constant under the load for the remaining 10 min at each location. A repeat of the load test was performed to investigate the initial response of the bridge to loading, and only nominal deformation was observed, importantly being elastic in nature (rebounding when the load was removed). The initial plastic settlement was hence determined to record the 'bedding-in' of the new work: by contrast, the pier itself exhibited zero deformation, which confirmed that the rebuilt skewback had bedded down into the pier. The repeat load test confirmed successful rehabilitation, and the bridge reopened to traffic (Figure 13).



Figure 13 The rehabilitated bridge opened to traffic following a successful load test

## 8. Summary and conclusions

- The structural behaviour of traditional masonry is an assemblage of dry-jointed masonry units drawing stability from its weight and geometry which governs thrust and counterthrust.
- Thrust-line equilibrium analysis was used to interpret rationally the possible load paths remaining in a seriously damaged structure.
- A complex 3D problem was broken down for assessment in two dimensions by traditional hand methods, the findings of which aligned with the observed structural pathology and gut feeling of the engineer.
- A phased approach to working proximity was successfully adopted, using real-time monitoring of structural movement, to ensure total workforce safety.
- A distinctive local landmark and heritage asset was saved from collapse and preserved in line with conservation engineering principles of compatible intervention, where the form, appearance and character of the original bridge were preserved.

## References

BSI 1986 BS 8004:1986: Code of practice for foundations BSI London, UK [Google Scholar](#)

BSI 2007 BS EN 1993-5:2007: Eurocode 3: Design of steel structures. Piling BSI London, UK [Google Scholar](#)

BSI 2009 BS 5228-2:2009: Code of practice for noise and vibration control on construction and open sites BSI London, UK [Google Scholar](#)

Cassinello M 2006 Effect of mortar joint thickness on deformability in medieval stone walls *Materiales de Construcción* 56 284 69 80 [Google Scholar](#)

Ciria (Construction Industry Research and Information Association) 1992 Ground-borne Vibrations Arising from Piling Ciria London, UK Technical Note 142 [Google Scholar](#)

Ciria 2006 Masonry Arch Bridges: Condition Appraisal and Remedial Treatment Ciria London, UK C656 [Google Scholar](#)

Ciria 2015 Manual on Scour at Bridges and Other Hydraulic Structures 2 Ciria London, UK [Google Scholar](#)

Cowper AD 1927 Lime and Lime Mortars Donhead Shaftesbury, UK [Google Scholar](#)

Cumbrian Stone 2016 Bowscar Sandstone Cumbrian Stone Penrith, UK See <https://cumbrianstone.co.uk/> (accessed 31/08/2017) [Google Scholar](#)

Curwen JF 1932 Parishes (West Ward): St Ninian, Brougham The Later Records Relating to North Westmorland or the Barony of Appleby Titus Wilson and Son Kendal, UK See <https://www.british-history.ac.uk/n-westmorland-records/vol8/pp278-290#h3-0011> (accessed 09/10/2018) [Google Scholar](#)

Harvey W 2011 Bridge of the Month No6 June 2011: Calva Bridge, Workington Obvis and Bill Harvey Associates Ltd Exeter, UK See <http://billharvey.typepad.com/BridgeOfTheMonth/Calva.pdf> (accessed 09/10/2018) [Google Scholar](#)

Harvey W 2012a The Coy Mistress – a view of masonry behaviour The Structural Engineer February 25 31 [Google Scholar](#)

Harvey W 2012b Stiffness and damage in masonry bridges *Proceedings of the Institution of Civil Engineers – Bridge Engineering* 165 3 127 134 [Link](#), [Google Scholar](#)

Harvey W 2013 A spatial view of the flow of force in masonry bridges *Proceedings of the Institution of Civil Engineers – Bridge Engineering* 166 1 51 58 <https://doi.org/10.1680/bren.11.00026> [Link](#), [Google Scholar](#)

Henry A Stewart J 2012 Mortars, Plaster & Renders English Heritage Swindon, UK [Google Scholar](#)

Heyman J 1969 The safety of masonry arches *International Journal of Mechanical Sciences* 11 363 365 [Crossref](#), [Google Scholar](#)

Heyman J 1982 The Masonry Arch Ellis Horwood Hemel Hempstead, UK [Google Scholar](#)

Heyman J 1996 Arches, Vaults and Buttresses Variorum Aldershot, UK [Google Scholar](#)

Highways Agency 1994 BA 54/94: Load testing for bridge assessment Highways Agency Guildford, UK [Google Scholar](#)

Highways Agency 2001 BD 37/01: Loads for highway bridges Highways Agency Guildford, UK [Google Scholar](#)

Historic England 2018a Brougham Castle Bridge Historic England London, UK See <https://historicengland.org.uk/listing/the-list/list-entry/1145357> (accessed 16/08/2018) [Google Scholar](#)

Historic England 2018b Brougham Roman Fort (Brocavum) and Civil Settlement and Brougham Castle Historic England London UK See <https://historicengland.org.uk/listing/the-list/list-entry/1007186> (accessed 16/08/2018) [Google Scholar](#)

Hume L 2014 The philosophy of conservation engineering Structures and Construction in Historic Building Conservation Forsyth M Wiley-Blackwell Chichester, UK 12 18 [Google Scholar](#)

Mathews R Hardman M 2017 Lessons learnt from the December 2015 flood event in Cumbria, UK Proceedings of the Institution of Civil Engineers – Forensic Engineering 170 4 165 178 <https://doi.org/10.1680/ifoen.17.00009> [Link](#), [Google Scholar](#)

McIntyre F 2018 Tech excellence: Brougham Old Bridge repairs New Civil Engineer March 14 50 52 See <https://www.newcivilengineer.com/tech-excellence/tech-excellence-brougham-old-bridge/10029147.article> (accessed 15/03/2018) [Google Scholar](#)

Page J 1996 A Guide to Repair and Strengthening of Masonry Arch Highway Bridges Transport Research Laboratory Wokingham, UK [Google Scholar](#)

Pavia S 2006 Repair mortars for masonry bridges Bridge and Infrastructure Research in Ireland: Symposium 2006 Nuallain N O'Connor A Gavin K Trinity College Dublin 183 190 [Google Scholar](#)

Ruddock T 2009 Arch Bridges and Their Builders 1735–1835 Cambridge University Press Cambridge, UK [Google Scholar](#)

Sowden AM 1990 The Maintenance of Brick and Stone Masonry Structures E. & F.N. Spon Cambridge, UK [Google Scholar](#)

Wiggins DE 2018a Masonry bridges and the importance of lime The Building Conservation Directory 2018 Taylor J 25 Cathedral Communications Wiltshire, UK 51 54 [Google Scholar](#)

Wiggins DE 2018b Hot-mixed Lime Mortars: Microstructure and Functional Performance Historic Environment Scotland Edinburgh, UK Technical Paper 27 [Google Scholar](#)

Wilmers W 2012 Restoration of masonry arch bridges Proceedings of the Institution of Civil Engineers – Bridge Engineering 165 3 135 146 <https://doi.org/10.1680/bren.11.00011> [Link](#), [Google Scholar](#)

**Published Online:** February 19, 2019  
<https://www.icevirtuallibrary.com/doi/10.1680/jenhh.18.00027>

## ΕΚΤΕΛΕΣΤΙΚΗ ΕΠΙΤΡΟΠΗ ΕΕΕΕΓΜ (2019 – 2022)

Πρόεδρος	:	Μιχάλης ΜΠΑΡΔΑΝΗΣ, Δρ. Πολιτικός Μηχανικός, ΕΔΑΦΟΣ ΣΥΜΒΟΥΛΟΙ ΜΗΧΑΝΙΚΟΙ Α.Ε. <a href="mailto:mbardanis@edafos.gr">mbardanis@edafos.gr</a> , <a href="mailto:lab@edafos.gr">lab@edafos.gr</a>
Α΄ Αντιπρόεδρος	:	Χρήστος ΤΣΑΤΣΑΝΙΦΟΣ, Δρ. Πολιτικός Μηχανικός, ΠΑΝΓΑΙΑ ΣΥΜΒΟΥΛΟΙ ΜΗΧΑΝΙΚΟΙ Ε.Π.Ε. <a href="mailto:editor@hssmge.gr">editor@hssmge.gr</a> , <a href="mailto:ctsatsanifos@pangaea.gr">ctsatsanifos@pangaea.gr</a>
Β΄ Αντιπρόεδρος	:	Μιχάλης ΠΑΧΑΚΗΣ, Πολιτικός Μηχανικός <a href="mailto:mpax46@otenet.gr">mpax46@otenet.gr</a>
Γενικός Γραμματέας:		Γιώργος ΜΠΕΛΟΚΑΣ, Δρ. Πολιτικός Μηχανικός, Επίκουρος Καθηγητής ΤΕΙ Αθήνας <a href="mailto:gbelokas@teiath.gr">gbelokas@teiath.gr</a> , <a href="mailto:gbelokas@gmail.com">gbelokas@gmail.com</a>
Ταμίας	:	Γιώργος ΝΤΟΥΛΗΣ, Πολιτικός Μηχανικός, ΕΔΑΦΟΜΗΧΑΝΙΚΗ Α.Ε.- ΓΕΩΤΕΧΝΙΚΕΣ ΜΕΛΕΤΕΣ Α.Ε. <a href="mailto:gdoulis@edafomichaniki.gr">gdoulis@edafomichaniki.gr</a>
Έφορος	:	Γεώργιος ΓΚΑΖΕΤΑΣ, Δρ. Πολιτικός Μηχανικός, Ομότιμος Καθηγητής Ε.Μ.Π. <a href="mailto:gazetas@central.ntua.gr">gazetas@central.ntua.gr</a> , <a href="mailto:gazetas50@gmail.com">gazetas50@gmail.com</a>
Μέλη	:	Ανδρέας ΑΝΑΓΝΩΣΤΟΠΟΥΛΟΣ, Δρ. Πολιτικός Μηχανικός, Ομότιμος Καθηγητής ΕΜΠ <a href="mailto:aanagn@central.ntua.gr">aanagn@central.ntua.gr</a> Παναγιώτης ΒΕΤΤΑΣ, Πολιτικός Μηχανικός, ΟΜΙΛΟΣ ΤΕΧΝΙΚΩΝ ΜΕΛΕΤΩΝ Α.Ε. <a href="mailto:otmate@otenet.gr">otmate@otenet.gr</a> Μαρίνα ΠΑΝΤΑΖΙΔΟΥ, Δρ. Πολιτικός Μηχανικός, Αναπληρώτρια Καθηγήτρια Ε.Μ.Π. <a href="mailto:mpanta@central.ntua.gr">mpanta@central.ntua.gr</a>
Αναπληρωματικά Μέλη	:	Χρήστος ΣΤΡΑΤΑΚΟΣ, Πολιτικός Μηχανικός, ΝΑΜΑ Α.Ε. <a href="mailto:stratakos@namalab.gr">stratakos@namalab.gr</a> Βάλια ΞΕΝΑΚΗ, Δρ. Πολιτικός Μηχανικός, ΕΔΑΦΟΜΗΧΑΝΙΚΗ Α.Ε. <a href="mailto:vxenaki@edafomichaniki.gr">vxenaki@edafomichaniki.gr</a>
Εκδότης	:	Χρήστος ΤΣΑΤΣΑΝΙΦΟΣ, Δρ. Πολιτικός Μηχανικός, ΠΑΝΓΑΙΑ ΣΥΜΒΟΥΛΟΙ ΜΗΧΑΝΙΚΟΙ Ε.Π.Ε. <a href="mailto:editor@hssmge.gr">editor@hssmge.gr</a> , <a href="mailto:ctsatsanifos@pangaea.gr">ctsatsanifos@pangaea.gr</a>

### ΕΕΕΕΓΜ

Τομέας Γεωτεχνικής  
ΣΧΟΛΗ ΠΟΛΙΤΙΚΩΝ ΜΗΧΑΝΙΚΩΝ  
ΕΘΝΙΚΟΥ ΜΕΤΣΟΒΙΟΥ ΠΟΛΥΤΕΧΝΕΙΟΥ  
Πολυτεχνειούπολη Ζωγράφου  
15780 ΖΩΓΡΑΦΟΥ

Τηλ. 210.7723434  
Τοτ. 210.7723428  
Ηλ-Δι. [secretariat@hssmge.gr](mailto:secretariat@hssmge.gr) ,  
[geotech@central.ntua.gr](mailto:geotech@central.ntua.gr)  
Ιστοσελίδα [www.hssmge.org](http://www.hssmge.org) (υπό κατασκευή)

«ΤΑ ΝΕΑ ΤΗΣ ΕΕΕΕΓΜ» Εκδότης: Χρήστος Τσατσανίφος, τηλ. 210.6929484, τοτ. 210.6928137, ηλ-δι. [ctsatsanifos@pangaea.gr](mailto:ctsatsanifos@pangaea.gr),  
[editor@hssmge.gr](mailto:editor@hssmge.gr), [info@pangaea.gr](mailto:info@pangaea.gr)

«ΤΑ ΝΕΑ ΤΗΣ ΕΕΕΕΓΜ» «αναρτώνται» και στην ιστοσελίδα [www.hssmge.gr](http://www.hssmge.gr)